A Section 508–conformant HTML version of this article is available at https://doi.org/10.1289/EHP8314.

Assessing the Association of Mitochondrial Function and Inflammasome Activation in Murine Macrophages Exposed to Select Mitotoxic Tri-Organotin Compounds

Gabrielle M. Childers,[1] Caroline A. Perry,[1†] Barbara Blachut,[1‡] Negin Martin,[2] Carl D. Bortner,[3] Stella Sieber,[4] Jian-Liang Li,[5] Michael B. Fessler,[6] and G. Jean Harry[1]*

[1]Molecular Toxicology Branch, National Institute of Environmental Health Sciences (NIEHS), National Institutes of Health (NIH), Department of Health and Human Services (DHHS), Research Triangle Park, North Carolina, USA
[2]Laboratory of Neurobiology, NIEHS, NIH, DHHS, Research Triangle Park, North Carolina, USA
[3]Signal Transduction Laboratory, NIEHS, NIH, DHHS, Research Triangle Park, North Carolina, USA
[4]Molecular Genomics Core Laboratory, NIEHS, NIH, DHHS, Research Triangle Park, North Carolina, USA
[5]Integrative Bioinformatics Support Group, NIEHS, NIH, DHHS, Research Triangle Park, North Carolina, USA
[6]Immunity, Inflammation, and Disease Laboratory, NIEHS, NIH, DHHS, Research Triangle Park, North Carolina, USA

Background: Mitochondrial function is implicated as a target of environmental toxicants and found in disease or injury models, contributing to acute and chronic inflammation. One mechanism by which mitochondrial damage can propagate inflammation is via activation of the nucleotide-binding oligomerization domain (NOD)-like receptor (NLR) family, pyrin domain-containing receptor (NLRP)3 inflammasome, a protein complex that processes mature interleukin (IL)-1β. IL-1β plays an important role in the innate immune response and dysregulation is associated with autoinflammatory disorders.

Objective: The objective was to evaluate whether mitochondrial toxicants recruit inflammasome activation and IL-1β processing.

Method: Murine macrophages (RAW 264.7) exposed to tri-organotins (triethyltin bromide (TETBr), trimethyltin hydroxide (TMTOH), triphenyltin hydroxide (TPTOH), bis(tributyltin)oxide) [Bis(TBT)Ox] were examined for pro-inflammatory cytokine induction. TMTOH and TETBr were examined in RAW 264.7 and bone marrow-derived macrophages for mitochondrial bioenergetics, reactive oxygen species (ROS) production, and inflammasome activation via visualization of aggregate formation, caspase-1 flow cytometry, IL-1β enzyme-linked immunosorbent assay and Western blots, and microRNA (miRNA) and mRNA arrays.

Results: TETBr and TMTOH induced inflammasome aggregate formation and IL-1β release in lipopolysaccharide (LPS)-primed macrophages. Mitochondrial bioenergetics and mitochondrial ROS were suppressed. *Il1a* and *Il1b* induction with LPS or LPS+ATP challenge was diminished. Differential miRNA and mRNA profiles were observed. Lower *miR-151-3p* targeted cyclic adenosine monophosphate (cAMP)-mediated and AMP-activated protein kinase signaling pathways; higher *miR-6909-5p*, *miR-7044-5p*, and *miR-7686-5p* targeted Wnt beta-catenin signaling, retinoic acid receptor activation, apoptosis, signal transducer and activator of transcription 3, IL-22, IL-12, and IL-10 signaling. Functional enrichment analysis identified apoptosis and cell survival canonical pathways.

Conclusion: Select mitotoxic tri-organotins disrupted murine macrophage transcriptional response to LPS, yet triggered inflammasome activation. The differential response pattern suggested unique functional changes in the inflammatory response that may translate to suppressed host defense or prolong inflammation. We posit a framework to examine immune cell effects of environmental mitotoxic compounds for adverse health outcomes. https://doi.org/10.1289/EHP8314

Introduction

Since the mid-1900s, an interest in the role of mitochondria in chemical-induced toxicity has developed primarily based on studies demonstrating alterations in oxidative phosphorylation following exposure to a heterogenous group of substances, including tri-organotin and tri-organolead compounds (Aldridge et al. 1977; Powers and Beavis 1991). This interest further developed with the implication of mitochondrial function as a target of environmental toxicants (Caito and Aschner 2015; Delp et al. 2019; Meyer et al. 2013; Shaughnessy et al. 2014; Xia et al. 2018). This, as well as work establishing mitochondrial deficits across various human diseases (Khan et al. 2015; Javadov et al. 2020) and modeled in the mouse (Wallace and Fan 2009) led to consideration of mitochondrial dysfunction as a key characteristic of toxicity and prompted the formulation of mitochondrial-based adverse outcome pathways (Dreier et al. 2019; Goodchild et al. 2019) for which causative links over the biological hierarchical processes are of current interest.

Increasing evidence suggests a role for metabolic remodeling by mitochondria in controlling the maintenance and establishment of innate and adaptive immune responses (Viola et al. 2019). Mitochondrial dysfunction occurs in many disease or injury models and is thought to propagate injurious inflammation through inducing mitochondrial reactive oxygen species (mtROS) and releasing endogenous mitochondrial damage-associated molecular patterns (DAMPs), which activate innate immune receptors (Nakahira et al. 2011; Zhou et al. 2011; Shimada et al. 2012), contributing to sustained inflammation (Dela Cruz and Kang 2018). Cross-communication between mitochondrial dysfunction and inflammation has been implicated owing to shared cellular processes (Johansson et al. 2010; Liu et al. 2018b; Mathur et al. 2018; Tschopp 2011). A central mechanism whereby damaged mitochondria propagate inflammation is the activation of the nucleotide-binding oligomerization domain (NOD)-like receptor (NLR) family, pyrin domain-containing receptor 3 (NLRP3) inflammasome. Inflammasomes are multiprotein complexes that involve the common adaptor, apoptosis-associated speck-like protein containing a caspase recruitment domain (CARD) apoptosis-associated speck-like protein containing a CARD (ASC), and an effector, caspase-1. In the cytosol of immune cells, this complex

Address correspondence to: G. Jean Harry, National Institute of Environmental Health, MD E1-07, 111 T.W. Alexander Dr., Durham, NC 27709 USA. Email: Harry@nih.gov

Supplemental Material is available online (https://doi.org/10.1289/EHP8314).

*Current address: Gabrielle M. Childers, University of Alabama at Birmingham, Birmingham, AL, USA.
†Current address: Caroline A. Perry, Perelman School of Medicine at the University of Pennsylvania, Philadelphia, PA, USA.
‡Current address: Barbara Blachut, Washington University School of Medicine, St. Louis, MO, USA.

The authors declare they have no actual or potential competing financial interests.

Received 18 September 2020; Revised 29 March 2021; Accepted 30 March 2021; Published 30 April 2021.

Note to readers with disabilities: *EHP* strives to ensure that all journal content is accessible to all readers. However, some figures and Supplemental Material published in *EHP* articles may not conform to 508 standards due to the complexity of the information being presented. If you need assistance accessing journal content, please contact ehponline@niehs.nih.gov. Our staff will work with you to assess and meet your accessibility needs within 3 working days.

forms in response to pathogen-associated molecular patterns or DAMPs that are released upon tissue injury and serves as a key sensor and effector of inflammation (Franchi et al. 2009; Ghiringhelli et al. 2009; Gross et al. 2011). Activated inflammasomes induce caspase-1-dependent processing of the pro-inflammatory cytokines interleukin (IL)-1β and IL-18 (Broz and Dixit 2016; Ghiringhelli et al. 2009), which play critical roles for host defense actions against invading factors and in coordinating the inflammatory response (Dinarello 2009; Sims and Smith 2010). The need to maintain this tightly regulated process is demonstrated in the number of inflammatory disorders or multifactorial diseases. NLRP3 inflammasome activation releases IL-1β for host defense actions that are critical to the overall health status of the organism. However, activation can also be associated with rare heritable inflammasomopathies and related diseases that cause excessive IL-1β activation and with a loss of immune regulation in common pathologies, such as cancer, cardiometabolic disease, neurological disorders, and diabetes (Dinarello 2011; Franchi et al. 2009; Kaneko et al. 2019; Swanson et al. 2019; Walsh et al. 2014). Thus, activation or dysregulation of this process can result in a broad spectrum of health effects underlying various disease processes.

Of the canonical inflammasomes, NLRP3 inflammasome is broadly sensitive to exogenous and endogenous activators. NLRP3 inflammasome activation generally requires prior transcriptional cell priming by an activating ligand. This priming step typically involves a nuclear factor kappa-light-chain-enhancer of activated B cells (NF-κB)-dependent) up-regulation of cellular NLRP3, pro-IL-1β transcription, and *de novo* protein synthesis upon recognition of pro-inflammatory stimuli and Toll-like Receptor (TLR) activation (Bauernfeind et al. 2009; Franchi et al. 2009). Once primed, NLRP3 activation can be induced by a variety of extracellular, sterile, nonpathogenic triggers (Cassel et al. 2009; Dostert et al. 2008; Hughes and O'Neill 2018; Strowig et al. 2012) that work through activating purinergic receptors or ionic membrane pore alterations (see the schematic representation in Figure 1). These sterile activators include cholesterol and uric acid crystals (Duewell et al. 2010; Martinon et al. 2006), aggregated proteins and lipids (Ralston et al. 2017; Sheedy et al. 2013), silica and asbestos (Dostert et al. 2008), aluminum salt adjuvant (Eisenbarth et al. 2008), and polystyrene nanoparticles (Lunov et al. 2011). In addition to these extracellular signaling factors, mitochondrial dysfunction may elicit an inflammasome response upon the release of mitochondrial DNA (Liu et al. 2018b). A number of molecules can directly or indirectly interact with different components of the NLRP3 inflammasome and impede complex assembly. In addition, negative regulatory molecules targeting ion efflux, mitochondrial function, and ROS signaling can block NLRP3 inflammasome

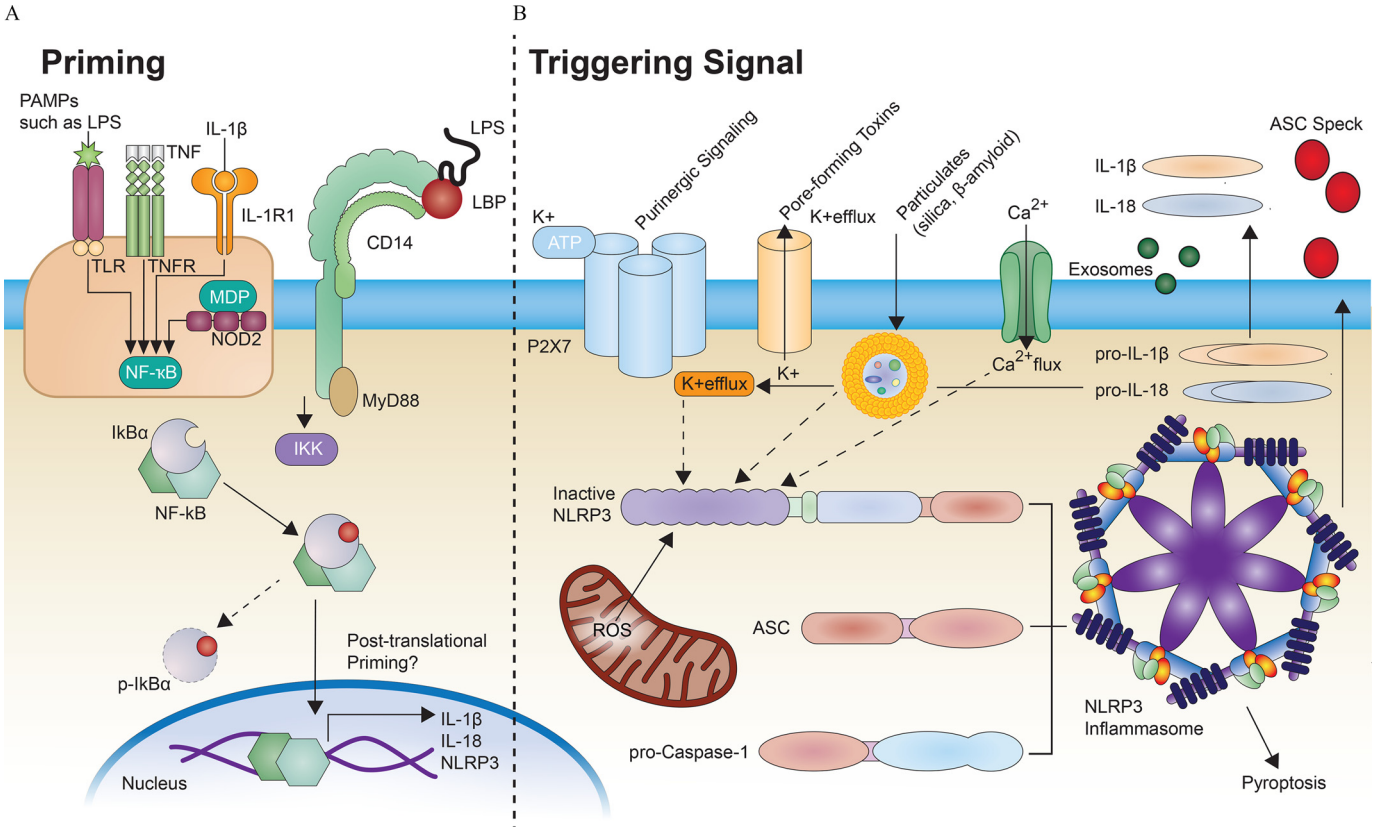

Figure 1. Representative schematic of NLRP3 inflammasome priming and activation (Deets and Vance 2021; Guo et al. 2015; Kelley et al. 2019; Martinon et al. 2002). The initial priming signal (A) is provided by activation of cytokines or pathogen-associated molecular patterns (PAMPs) and signaling through Toll-like receptors (TLRs), tumor necrosis factor receptors (TNFRs), and the IL-1 receptor 1 (IL-1R1), lipopolysaccharide (LPS), resulting in transcriptional up-regulation of canonical and noncanonical NLRP3 inflammasome components. The second, triggering, signal (B) then serves to trigger the response and can be provided by any number of PAMPs or damage-associated molecular patterns (DAMPs). These include pore-forming toxins to allow K^+ efflux, particulates and crystals (β-amyloid, uric acid, silica) that are taken up into the lysosome, and adenosine triphosphate (ATP) as a purinergic type 2 receptor 7 (P2X7) ligand. These signals can activate multiple signaling events such as K^+ efflux, Ca^{2+} flux, lysosomal disruption, and mitochondrial reactive oxygen species (ROS) production, which can lead to NLRP3 inflammasome activation (dashed arrows). Oligomerization of the components to form the inflammasome activates caspase-1 that then cleaves pro-IL-1β and pro-IL-18. Activation leads to the release of mature IL-1β and IL-18, pore formation, pyroptosis, and/or release of exosomes or ASC specks. Note: ASC, apoptosis-associated speck-like protein containing a caspase recruitment domain; ATP, adenosine triphosphate; IκBα, nuclear factor of kappa light polypeptide gene enhancer in B-cells inhibitor, alpha; p-IκBα, phosphorylated IκBα; Iκκ, inhibitor of nuclear factor-κB kinase; IL, interleukin; LBP, lipopolysaccharide binding protein; MDP, muramyl dipeptide; NLRP3, nucleotide-binding oligomerization domain-like receptor family, pyrin domain-containing receptor 3.

activation (Zheng et al. 2020). Thus, in addition to functioning as a direct activator, changes in mitochondrial function or induction of ROS can serve as underlying cellular mechanisms for NLRP3 activation induced by multiple, disparate triggering stimuli (Nakahira et al. 2011; Shimada et al. 2012; Tschopp and Schroder 2010; Zhou et al. 2011).

Given the complex interaction between mitochondria and inflammation, we hypothesized that mitochondrial dysfunction induced by environmental toxicants represents a mechanism leading to altered immune cell functioning and that triggering of the NLRP3 inflammasome serves as one step along the biological pathway leading to an adverse health outcome. Chemical-induced alterations in mitochondrial membrane potential (MMP) have been used to identify mitochondrial toxicants by Tox21 screening (Attene-Ramos et al. 2015). We considered whether they may be further classified based upon NLRP3 inflammasome activation and IL-1β production and thus provide a better characterization. To examine this possible association, a class of compounds were selected based upon effects on oxidative phosphorylation and immune cell stimulation/dysfunction and with evidence of *in vivo* toxicity. Several of the tri-organotins, triphenyltin (TPT), triethyltin (TET), trimethyltin (TMT), and tributyltin (TBT), met the criteria of altered mitochondrial (Aldridge et al. 1977; 1981; Davidson et al. 2004; Gennari et al. 2000; Nesci et al. 2011; Powers and Beavis 1991; Snoeij et al. 1987) and human and murine immune cell functions (Benya 1997; Brown et al. 2018; Ferraz da Silva et al. 2018; Gomez et al. 2007; Lawrence et al. 2016; Nunes-Silva et al. 2018; Pestka and Zhou 2006; Van Loveren et al. 1990; Whalen et al. 1999; Wu 2019). For example, altered immune function has been reported for TBT with decreased peripheral lymphocytes (Attahiru et al. 1991; Snoeij et al. 1988; Ueno et al. 2009) and thymus atrophy (Snoeij et al. 1988) in rats, T-cell development in mice (Im et al. 2015), macrophage phagocytic activity, intestinal mucosal immune response, and B-lymphocyte proliferation in cod (Harford et al. 2007), and antibody production to immune challenge in catfish (Regala et al. 2001). TPT and/or TMT disrupted lytic function of human natural killer cells *in vitro* (Gomez et al. 2007; Holloway et al. 2008) and delayed-type hypersensitivity reactions in rats (Snoeij et al. 1985) and exacerbated a pro-inflammatory response in lipopolysaccharide (LPS)-primed murine macrophages (Pestka and Zhou 2006). TMT and TET demonstrated an inflammatory component associated with neurotoxicity in rodent models (Harry et al. 2003; Kraft et al. 2016; Long et al. 2019; Röhl et al. 2009; Sandström et al. 2019). The implication of immunodeficiency following TBT exposure and the stimulation of neuroimmune cells with TET and TMT, as well as the documented effects on oxidative phosphorylation, suggested the possibility that, in the absence of a direct effect, an inflammatory response could be elicited by alternative processes, such as inflammasome activation. Given the critical role of macrophage-type cells in immune-related responses, we examined the ability of these selected tri-organotins to serve as secondary triggers for NLRP3 inflammasome activation and IL-1β processing. We further examined cells for mitochondrial dysfunction, ROS production, and microRNA (miRNA) and mRNA gene expression profiles to characterize differences across the two tri-organotin compounds—TET and TMT—to investigate the potential to trigger mature IL-1β release.

Methods

Exposure Chemical Solutions

Stocks of 40 μM trimethyltin hydroxide [TMTOH; 98% Chemical Abstract Service Registry Number (CASRN) 56-24-6; #71167], 400 μM triethyltin bromide (TETBr; 97%, CASRN 2767-54-6; #71135; Alfa Aesar), triphenyltin hydroxide (TPTOH; 96%, CASRN 76-87-9; #348104), or bis(tributyltin) oxide [Bis(TBT)Ox; 96%, CASRN 56-35-9; #B353383, Sigma-Aldridge] in phosphate buffered saline (PBS) were calculated on the basis of the molecular weight of the form of tin. Stocks were stored at 4°C. Stocks of ultrapure LPS (*Escherichia coli* O111:B4; #421; Lot #4217A1; 2.6 EU/ng; List Biologicals) were sonicated in PBS, adenosine 5′-triphosphate disodium salt hydrate (ATP; 100 mM, A46419; Sigma-Aldridge), suspended in sterile dH_2O, and stored at −20°C. Final solutions were prepared immediately prior to experiment.

Cell Cultures

RAW 264.7 cells [American Type Culture Collection (ATCC) Catalog no. TIB-71, RRID:CVCL_0493] are BALB/c murine cell line derived from males. Cells at <15 passages, within a stable range for gene expression (Taciak et al. 2018), were maintained in Dulbeccos's Modified Eagle's Medium (DMEM; L-glutamine and sodium pyruvate; #11995-065 Gibco; ThermoFisher) supplemented with 10% fetal bovine serum (FBS; <0.25 EU/mL; Catalog no. 100-108; Lot #A22GOOJ; Gemini Bio-Products) and 100 U/mL penicillin/streptomycin (#P0781; Sigma-Aldrich). Unless otherwise stated, cells were plated in tissue culture plates (Corning) at 20,000 cells/well (62,500 cells/cm^2; 96-well); 300,000 cells/well (150,000 cells/cm^2; 24-well); 1,000,000 cells/well (105,000 cells/cm^2; 6-well) and allowed to adhere overnight prior to experimental manipulation. Cells were not allowed to become more than 80% confluent in order to prevent loss of the flattened adherent cell characteristic. Cells were maintained at 37°C, 5% CO_2/5% O_2, 90% humidity (Nu-5831 tri-gas incubator; Nuaire). Immediately prior to dosing, media volume was decreased by 50%. Corning black-walled optical plates were used for fluorescent imaging.

Primary Bone Marrow-Derived Macrophages

C57BL/6J male mice (6- to 12-wk-old; IMSR Catalog no. JAX:000664, RRID:IMSR_JAX:000664) were euthanized under CO_2, the femur excised, bone marrow extruded, and primary bone marrow-derived macrophages (BMDMs) collected (Trouplin et al. 2013). Animals were handled in accordance with the National Institutes of Health *Guide for the Care and Use of Laboratory Animals* following an approved animal protocol from the National Institute of Environmental Health Sciences Animal Care and Use Committee. Isolated cells were initially plated 1,000,000 cells/well per 12-well plate in 3 mL DMEM (Gibco #11965-092; 10% FBS, 100 U/mL penicillin/streptomycin) supplemented with 10% L929 DMEM conditioned-media (CM) as a source of macrophage colony stimulating factor to induce hematopoietic cell differentiation into macrophages. Cells were allowed to adhere at 37°C, 5% CO_2/5% O_2, 90% humidity (Nu-5831 tri-gas incubator; Nuaire), followed by half DMEM/CM change on days *in vitro* 3 (DIV3) and full change to DMEM on DIV5 to remove nonmacrophage contaminating cells. On DIV6, a half-media change occurred with tri-organotin addition.

Exposure Levels

Human levels for TBT and TPT have been detected in the nanograms-per milliliter range (TBT ranging in whole blood between <0.01 and 85 and in serum between <0.02 and 0.05; TPT in whole blood between <0.4 and 0.56 and in serum between 18 and 0.67) (Sousa et al. 2014). Occupational exposure to TMT in 216 factory workers (personal air sampling over 8 h detected between 0.008 and 0.028 mg TMT/m^3) resulted in the detection of TMT in 61 workers ranging up to 0.264 μg/mL in plasma and 211.8 mg/g creatine in urine (Tang et al. 2013). The

limited data available for TET estimated the toxic dose for an adult to be ~70 mg of TET over 8 d (Barnes and Stoner 1959) and in children, ~4.5 mg (Fontan et al. 1955). *In vitro* assessments of these tri-organotins included primary human cortical neurons or astrocytes after 24-h exposure to 10^{-3}M TMTBr or 10^{-5}M TETCl, maintaining >80% viability (Cristòfol et al. 2004). In primary hippocampal neurons, normal viability was maintained over 24 h with 1 μM TMT (Hou et al. 2017). In primary rat microglia, median lethal concentration values of 24.8 μM for TMT, 4.3 μM for TET, and 0.7 μM for TBT with 24 h were determined, with 80% viability observed at 2 μM TMT or 1 μM TET (Röhl et al. 2009). In LPS-primed RAW 264.7 cells, 6-h exposure to 1 μM TPT decreased *Tnfa* but not cell viability (Pestka and Zhou 2006) and Sandström et al. (2019) reported normal cell viability and an increase in *Il6* and *Inos* in BV-2 cells at 1 μM TMTCl for 24 h and limited alterations in three-dimensional brain cell cultures with 0.5 or 1 μM for 10 d.

Exposure levels were empirically determined using multiple doses (0.6–60 μM) over 24 h for a criterion of cell viability >75% to ensure that the responses observed would not be directly related to cell death. Final concentrations were selected based on empirically determined >75% cell viability and normal cell morphology. Exposure concentrations were calculated based on compound species. For example, TETBr (10 μM = 2.8 μg/mL = 2 μgTET/mL), TMTOH (1.25 μM = 0.226 μg/mL = 0.2 μgTMT/mL), Bis-(TBT) Ox (30 μM = 17.8 μg/mL = 8.7 μgTBT/mL), TPTOH (20 μM = 7.3 μg/mL = 4.7 μgTPT/mL).

Cell Exposure

To examine the direct effects of tri-organotins, cells were exposed to vehicle (PBS), TETBr, TMTOH, Bis(TBT)Ox, or TBTOH. In the inflammasome activation paradigm, cells were primed with LPS (RAW 264.7: 33 ng/mL; BMDM: 50 ng/mL) for 3 h and followed by PBS, TETBr (10 μM) or TMTOH (1.25 μM) for 6 h or 16 h. ATP (5 mM; 30 min) served as the positive trigger. To determine whether the tri-organotins altered the inflammatory response to LPS, RAW 264.7 cells were exposed to TETBr (10 μM) or TMTOH (1.25 μM) for 6 h prior to LPS challenge (33 ng/mL; 3 h). Additional examinations were conducted to confirm whether lower dose levels of TETBr (1.0 μM = 0.2 μg/mL) or TMTOH (0.06 μM = 0.01 μg/mL) would also serve as a secondary inflammasome trigger and to determine whether 18-h exposure to TETBr (1.0 μM = 0.2 μg/mL) or TMTOH (0.05 μM = 0.009 μg/mL) altered the ATP-triggered NLRP3 inflammasome response [LPS (33 ng/mL; 3 h), then ATP (5 mM; 30 min)].

Cell Viability

Cell viability was determined using CyQuant Direct Cell Proliferation Assay (C35013; Molecular Probes). Cells were incubated with CyQuant reagent (37°C; 60 min) and measurements read at 508 nm excitation/562 nm emission (BioTek Synergy four-plate reader). The live cell number was estimated based upon a standard curve and calculated as the percentage of the control. Cell viability of ~75–85% was used to select dose levels for further study.

Mitochondrial Membrane Potential

MMP was determined using the JC-10 assay (52305, Enzo Life Sciences). Briefly, cells were incubated for 40-min in 25 μM JC-10 in 20 mM 2-[4-(2-hydroxyethyl)piperazin-1-yl]ethanesulfonic acid (HEPES) buffer, rinsed, 50 μL HEPES/PBS were added, and measurements were taken at 510/530 and 510/590 (CLARIOStar plate reader; BMG Labtech). Fluorescence localization was confirmed using a Nikon TE2000-E microscope. Data was calculated as a ratio of 530:590 readings and presented as relative to the 10-μM antimycin maximum response.

RNA Isolation and Real-Time Polymerase Chain Reaction

Total RNA was isolated using TRIzol Reagent (Invitrogen), assessed by NanoDrop (Thermos Scientific), and complementary deoxyribonucleic acid (cDNA) synthesized from 2.5 μg total RNA using SuperScript II reverse transcriptase with random hexamers (Invitrogen). Real-time quantitative polymerase chain reaction (qPCR) was performed in duplicate using a 7900HT Fast Real-Time PCR System (Applied Biosystems). cDNA (3 μL) served as a template with normal working concentration Power TaqMan Universal PCR Master Mix (ThermoFisher) and normal working concentration TaqMan Gene Expression Assays [*Tnfa* (Mm00443258_m1), *Il1a* (Mm00439620_m1), *Ilb* (Mm00434228_m1), Tlr4 (Mm00445273_m1), *Arg2* (Mm00477592_m1), and *Il10* (Mm001288386_m1), *P2rx7* (Mm01199500_m1), *P2rx4* (Mm00501787_m1), *A20* 1380 (Mm00437121_m1), and *Gapdh* (Mm99999915_g1)]. The 20-μL reaction mixtures were held at 50°C/2 min, 95°C/10 min, followed by 40 cycles at 95°C/15 s, then 60°C/1 min. Amplification curves were generated with QuantiStudio 6 and 7 Flex Real-Time PCR System software (Applied Biosystems). Relative mRNA amounts were calculated using a normalized standard curve and expressed as ratios of the target gene to glyceraldehyde 3-phosphate dehydrogenase (GAPDH). In the present study, we found no significant differences in *Gapdh* across groups, suggesting a higher level of expression stability under these experimental conditions (Excel Table S1). Data met the inclusion criteria of transcript detection at <32 cycles.

Tumor Necrosis Factor-α and IL-1β enzyme-linked immunosorbent assay

Mouse tumor necrosis factor-α (TNFα) ELISA MAX kits (#430901; Lot #B257152, BioLegend) and IL-1β enzyme-linked immunosorbent assay (ELISA; #559603; Lot #4303741; BD Biosciences) with BD OptEIA Reagent Set B were used for analysis of RAW 264.7 cell supernatants (1 mL total supernatant; 1×10^6 cells/6-well plate). Briefly, capture antibodies (100 μL; 1:250) were held overnight at 4°C, washed with buffer, then held at room temperature (RT) for 1 h. A 100-μL sample aliquot was added for IL-1β or 100 μL of a sample aliquot diluted 40× for TNFα and incubated (RT; 2 h). Wells were washed and 100 μL detection antibody (1:500) added (RT; 1 h), and washed again, followed by adding 100 μL streptavidin-horseradish peroxidase (HRP) antibody (1:250; RT; 30 min) and 100 μL substrate solution (RT; dark; 30 min) then 50 μL stop solution. Optical density values were determined at 450 nm with a 570 nm background subtraction in a BioTek Synergy four-plate reader. Protein levels were calculated based on a standard curve.

IL-1 Release

HEK-Blue IL-1R cells (hkb-il1r; InvivoGen) were used to determine IL-1 release by RAW 264.7 cells. Briefly, HEK-Blue cells (50,000 cells/well per 96-well plate), a 20-μL aliquot RAW 264.7 cell media (total 1 mL/6-well plate), and 180 μL DMEM (4.5 g/L glucose, 2 mM L-glutamine, 10% heat inactivated FBS, 50 U/mL penicillin, 50 μg/mL streptomycin, 100 μg/mL Normocin, 200 μg/mL hygromycin B Gold, 1 μg/mL puromycin, and 100 μg/mL Zeocin) were incubated overnight at 37°C. Wells devoid of cells served as background controls. A 20-μL aliquot of the supernatant was incubated with 180 μL Quanti-Blue (InvivoGen) (37°C; 1 h; 96-well enzymatic plate). Absorbance measurements at 630 nm were recorded (BioTek Synergy four-

plate reader). Data was calculated relative to the background control.

IncuCyte Tracking of ASC Oligomerization

ASC speck formation has been effectively used as a readout for inflammasome activation (Stutz et al. 2013). Real-time imaging of NLRP3 inflammasome aggregate assembly was conducted using a RAW 264.7-ASC reporter cell line, as previously described (Bowen et al. 2020). HEK293T/17 cells (ATCC #CRL-11268; RRID: CVCL_1926) were transiently transfected with pMD2G (RRID: Addgene_12259), pUMVC (RRID:Addgene_8449) and retroviral transfer vector pRP-ASC-ESCBLerulean (RRID:Addgene_41840) using Invitrogen Lipofectamine 2000 (#1168019; ThermoFisher) (Barde et al. 2010). To determine titers (transducing units per milliliter), HEK293Ts cells (50,000 cells/well 6-well plate) were incubated at 37°C, 5% CO_2 for 24 h. The media was replaced and 10 μL of nonconcentrated or 0.5 μL of concentrated virus added. The media was replaced at 24 and 72 h after infection. At 5-d postinfection, chromosomal DNA was isolated using DNeasy Blood and Tissue Kit (#69506; Qiagen), diluted 1:40, and 5 μL diluted DNA was used in qPCR. Diluted retro/lentiviral plasmids and human genomic DNA were used to create standard curves for qPCR analysis. The following primers for gag (lentiviruses, forward: 5′-GGAGCTAGAACGATTCGCAGTTA; and reverse: 5′-GGTTGTAGCTGTCCCAGTATTTGTC), psi (retroviruses, forward: 5′-GCAGCATCGTTCTGTGTTGT; and reverse: 5′-GCTCGACATCTTTCCAGTGA), and actin (forward: 5′-TCCGTGTGGATCGGCGGCTCCA; and reverse 5′-CTGCTTGCTGATCCACATCTG) were used to with SYBR green to perform qPCR using Roche LightCycler 96 Instrument, and LightCycler 96 software was used to extrapolate the copies of gag/psi and actin per sample. In addition, the cells were fixed in 1% formalin and flow cytometry (BD LSRFortessa cell analyzer) was used to determine the percentage of fluorescent cells. Gag/psi copies relative to actin copies/two per cell were calculated and the titer was determined per copies in 100,000 cells times the virus dilution factor. Post-48-h transfection-supernatant was used for the transduction of RAW 264.7 cells (Stutz et al. 2013). Cell culture conditions were identical to normal RAW 264.7 cells. Cells were exposed to PBS or LPS (33 ng/mL) for 3 h, then to TETBr (10 μM), TMTOH (1.25 μM), or ATP (5 mM). To eliminate extracellular ATP and inhibit activation of purinergic receptors (P2XRs), apyrase (5 U/mL), an enzyme that converts ATP to ADP, was added to each well 1 h prior to organotin. Time-lapse images were obtained using an IncuCyte S3 live-cell analysis system (20-manification objective) (Sartorius) by IncuCyte ZOOM 2015A software and formation of ASC aggregates was determined (Stutz et al. 2013). Regions of interest (ROI) images were standardized by total number of cells, and threshold for ASC speck size and intensity, and ASC speck number was determined using Fiji ImageJ (Schindelin et al. 2012).

Flow Cytometry for Active Caspase-1

RAW 264.7-ASC cells (300,000 cells; 24-well plate) were incubated with FAM-FLICA Caspase-1 dye (10 μL; 1:30 PBS; 2 h; #98; Lot #15L23; Immunochemistry Technologies), rinsed in PBS, followed by 150 μL 10-times normal working concentration trypsin/ethylenediaminetetraacetic acid for 2 min, then 150 μL DMEM/20% FBS. Cells and the rinse were centrifuged ($250 \times g$, 5 min, 4°C), then rinsed two times, resuspended in 300 μL cold wash buffer, and kept on ice for 30 min. Cells were co-labeled with propidine iodide (PI; #P3566; Invitrogen; 1.0 mg/mL). Population analysis was conducted [BD LSRII flow cytometer (BD Biosciences) with gating parameters (BD FACSDiva software; Figure S3]. FAM-FLICA Caspase-1 was excited (488 nm laser) and detected using a 530/30 nm filter. For each sample, 10,000 cells were analyzed, gating initially on forward-scatter area vs. height dot plot, then forward-scatter vs. side scatter dot-plot excluding debris. Single FAM-FLICA Caspase-1^+ cells were examined to determine the shift in the positive cell population.

Western Blot for IL-1β

RAW 264.7 ASC cells (6×10^6 cells) in 6 mL serum-free DMEM were incubated with LPS for 3 h, then with PBS, TMTOH (1.25 μM), or TETBr (10 μM) for 6 h, or ATP (5 mM; 30 min). The media (supernatant) was collected, and the cells were lysed with 150 μL radioimmunoprecipitation assay buffer (Santa Cruz Biotechnology; 1 mM phenylmethylsulfonyl fluoride, 2 mM sodium orthovanadate) for 30 min on ice, vortexing at 10-min intervals. A 1.5-mL aliquot was concentrated by 3K centrifugal filters (Millipore). Protein concentrations were determined by Pierce bicinchoninic acid (BCA) assay (ThermoFisher). Samples (supernatant: 400 μg protein; cell lysate: 90 μg protein) were added to 50 μL streptavidin magnetic beads (Pierce) and 1.25 μg biotinylated polyclonal goat antimouse IL-1β (R&D Systems) to a volume of 400 μL with Tris-buffered saline/0.1% Tween 20 and incubated overnight at 4°C with mixing. The beads were washed three times, the protein was eluted with 30 μL Pierce IgG elution buffer (21004; ThermoFisher), and the protein precipitates were resuspended in 10 μL sample buffer (4× lithium dodecyl sulfate and 10× reducing agent) (Life Technologies) and subjected to gel-electrophoresis [Mini-Protean TGX Stain-Free 4–20% gels (BioRad) (200 mV; 30 min; Mini-PROTEAN Tetra Cell System)]. Proteins were wet-transferred (45 V; 60 min) to activated 0.2-μm nitrocellulose membranes (BioRad), then incubated with polyclonal goat antimouse IL-1β (AB-401-NA; R&D Systems; RRI: AB_354347;1:2,500; 1 μg/mL) in 5% low-fat milk at 4°C, overnight. Rinsed membranes were incubated with IRDye 800CW donkey antigoat (LICOR; 1:10,000; 0.1 μg/mL in 5% low-fat milk) for 1 h at RT. IL-1β bands (pro-37 kD; mature-17 kD) were detected using LICOR Odyssey, and densities were determined using Image Studio (LICOR). Levels of each density were calculated relative to the total IL-1β in each lane. For BMDM, a 500-μL aliquot of media from 2×10^6 cells was sequentially subjected to 50K and 3K centrifugal filters (Millipore), and the membranes were incubated with rabbit antigoat IgG-HRP (Santa Cruz;1:2,500; 5% low-fat milk; 1 h; RT), and protein bands were detected using Clarity ECL (Bio-Rad) and captured using an Azure Biosystems C300 imager with densitometric values determined by cSeries Capture software.

Nitrite Production

Nitrite accumulation in culture medium was measured as an indirect indicator of nitric oxide synthesis using a GREISS Reagent kit (G2930; Lot #122106; Promega). Briefly, a 50-μL aliquot of 100 μL phenol-free cell media and 50 μL sulfanilamide were held (RT; dark; 10 min), followed by 50 μL *N*-1-napthylethylenediamine (RT; dark; 10 min). Absorbance at 548 nm was recorded (BioTek Synergy four-plate reader). Background-corrected data was calculated relative to a sodium nitrite standard curve.

Immuno-Spin Trapping

5,5-Dimethyl-1-pyrroline *N*-oxide (DMPO) reacts with secondary radicals to form nitrone adducts that remain covalently attached as radical reporters and immune-spin trapping allows for stabilization for antibody identification (Ramirez and Mason 2005). DMPO-tagged secondary radicals were determined in whole-cell fractions and mitochondrial fractions of RAW 264.7

cells. Cells were expanded to 80–90% confluency in a T75 flask. Media was changed to serum-free DMEM media containing 40 mM DMPO (D048; Lot #GB635; Donjindo Molecular Technologies) for 30 min prior to exposure to either PBS, TMTOH, or TETBr for 6 h. Cells were detached with 0.25% trypsin, centrifuged ($200 \times g$; 10 min; RT), rinsed, and resuspended in 1 mL PBS. A 200-μL cell lysate aliquot was collected and stored at −80°C for <2 d. Mitochondria was isolated by differential centrifugation (Darley-Usmar et al. 1987). Cells were resuspended in ice-cold mitochondria isolation buffer {10 mM HEPES (pH 7.4), 250 mM sucrose, 10 mM 2-[2-[2-[2-[bis(carboxymethyl)amino]ethoxy]ethoxy]ethyl-(carboxymethyl)amino]acetic acid (pH 7.4), and 5 mg/mL bovine serum albumin (BSA)}. The solution was transferred into a chilled 0.15-mm Dounce tissue homogenizer and after 12 strokes at 600 rpm, cellular debris and unbroken cells were pelleted from the solution by centrifugation at $1{,}000 \times g$ for 10 min at 4°C. Cellular debris and unbroken cells were pelleted from the solution by centrifugation ($500 \times g$; 10 min; 4°C). The supernatants, containing isolated mitochondria, were transferred into a new tube and centrifuged for 10 min at $10{,}000 \times g$ and 4°C. The pellets containing isolated mitochondria were washed once with ice-cold isolation buffer without BSA. The final mitochondrial pellet obtained was resuspended in the isolation buffer containing protease inhibitors and kept on ice. Eight hundred-microliter mitochondrial aliquots were centrifuged ($200 \times g$; 10 min; RT), and the pellets were stored at −80°C for <2 d. Protein concentrations were determined by Pierce BCA assay (ThermoFisher). Nitrone adducts were detected by DMPO ELISA (Ramirez and Mason 2005; Taetzsch et al. 2015). Briefly, a 96-well ELISA plate (NUNC MaxiSorp; ThermoFisher Scientific) was coated with the sample (100 μg/well) at 4°C overnight. The plate was blocked with a 1% casein solution (Sigma-Aldridge) and 5% sucrose in PBS for 2 h. Anti-DMPO (1:1,000 in 1% casein/PBS) was applied for 1 h, washed three times with PBS, followed by HRP-antirabbit (1:1,000 in 1% casein/PBS). The wells were washed three times with PBS and 3,3′,5′5-tetramethylbenzidine liquid substrate (100 μL; Sigma-Aldridge) was applied for 20 min. The reaction was stopped with 50 μL of 2N sulfuric acid solution, and the plate was read at 450Å on a Tecan plate reader (Tecan US).

Seahorse Flux Analyzer

Cells were plated in a Seahorse XF96 microplate (25,000 cells/well; 80 μL DMEM/10% FBS/antibiotics; Agilent Technologies) and allowed to adhere for 1 h, then incubated for 20 h under standard conditions. Cells were exposed to PBS, TETBr (1.25 or 10 μM), or TMTOH (1.25 μM) for 6 h. The media was removed and replaced with 180 μL Seahorse XF media supplemented with 4.5 g/L glucose, 2 mM L-glutamine, and 1 mM sodium pyruvate (pH 7.4) and maintained under ambient air conditions at 37°C for 1 h. Oxygen consumption rates (OCRs) were measured using an XF96 Extracellular Flux Analyzer (Agilent Technologies). Sensor cartridges delivered a final concentration of 0.9 μM oligomycin, 0.75 μM carbonyl cyanide-4-(trifluoromethoxy)phenylhydrazone (FCCP), and 1 μM rotenone for the mitochondrial stress test using Agilent Wave software (version 2.4.0). Prior to and immediately following the assay, cells were visualized by light microscopy to confirm cell viability and culture uniformity.

miRNA and mRNA Arrays

Based on the comparable ability to serve as a secondary trigger for mature IL-1β release, we examined the response of primary LPS-primed BMDMs to a 6-h exposure to TMTOH (1.25 μM) or TETBr (10 μM) for associated molecular profiles. Total RNA was isolated from three samples (6×10^6 cells) using TRIzol (Invitrogen), treated with 2.5 μL DNase I and 10 μL Buffer RDD (#79254, RNase-Free DNase Set; Qiagen) (RT; 10 min), followed by column separation (#74104, RNeasy mini prep; Qiagen). miRNA analysis was conducted using Affymetrix GeneChip (version 4; Affymetrix) following the Affymetrix hybridization protocols. Total RNA (110 ng) was labeled using Affymetrix FlashTag Biotin HSR, according to the manufacturer's protocol. On average, 14.1 μg of labeled sample was hybridized (16 h; 48°C) in a rotating hybridization oven using Affymetrix Eukaryotic Target Hybridization Controls and protocol. On the same samples, mRNA analysis was conducted using Affymetrix Mouse Genome 430 2.0 GeneChip arrays (Affymetrix). Total RNA (50 ng) was amplified (Nugen WT-Ovation Pico RNA Amplification System) and labeled (Nugen Encore Biotin Module protocol). Amplified biotin–cDNAs (5.5 μg) were fragmented and hybridized (16 h; 45°C). Slides were stained with streptavidin/phycoerythrin using a double antibody staining procedure and then washed for antibody amplification (GeneChip Hybridization; Wash and Stain Kit). Arrays were scanned (Affymetrix Scanner 3000) and data were obtained using Transcriptome Analysis Console software (version 4.0).

miRNA and RNA Expression Array Data Analysis

miRNA data were preprocessing and normalized using Affymetrix Expression Console (build 1.4.1.46). Only mouse miRNAs were retained for downstream analysis. The mouse Genome 430 array data were preprocessing and normalized using the Affymetrix package. The Robust Multichip Analysis (RMA) approach was applied for normalization. To identify differentially expressed miRNAs and mRNAs, the empirical Bayes moderated *t*-statistics method implemented in the limma package (Ritchie et al. 2015) was performed. The fold-change differences of probe-sets expression were calculated based on normalized $\log_2$-transformed RMA values. *p*-Values were adjusted (Benjamini and Hochberg 1995) to control false discovery rate and correct for multiple hypothesis testing. miRNAs with a $p \leq 0.05$ and absolute fold-change >1.5 and mRNA probe sets with an adjusted $p \leq 0.05$ and absolute fold-change >2 were considered as differentially expressed. Predicted and validated miRNA-binding sites of known genes were determined using miRWalk (http://mirwalk.umm.uni-heidelberg.de) and miRDB (http://mirdb.org) programs. Targeted enrichment analyses were carried out with Qiagen Ingenuity Pathway Analysis software to test for pathway or functional group in significantly differentially expressed genes. Nontargeted enrichment analysis was conducted by gene set enrichment analysis to evaluate whether genes in a gene set were enriched at the top or bottom of the entire expression data as ranked by fold-change. Statistical analyses were performed using R/Bioconductor. Data were deposited in the National Center for Biotechnology Information Gene Expression Ominbus (GSE155128).

Statistical Analysis

Statistical analyses were performed using GraphPad Prism software (version 8.4, GraphPad Software, Inc.). In experiments where ATP or LPS were used as assay positive controls, that data was not included in the analyses. Data from experiments comparing across tri-organotin exposure in non-LPS-primed cells were evaluated using a one-way analysis of variance (ANOVA). Data from experiments examining the response of cells to LPS following tri-organotin exposure or in assessing the response to tri-organotins in LPS-primed cells were analyzed by a two-way ANOVA with tri-organotin and LPS as factors. ASC speck formation was analyzed by repeated measures ANOVA. Independent group mean comparisons were conducted with Tukey's or Dunnett's multiple

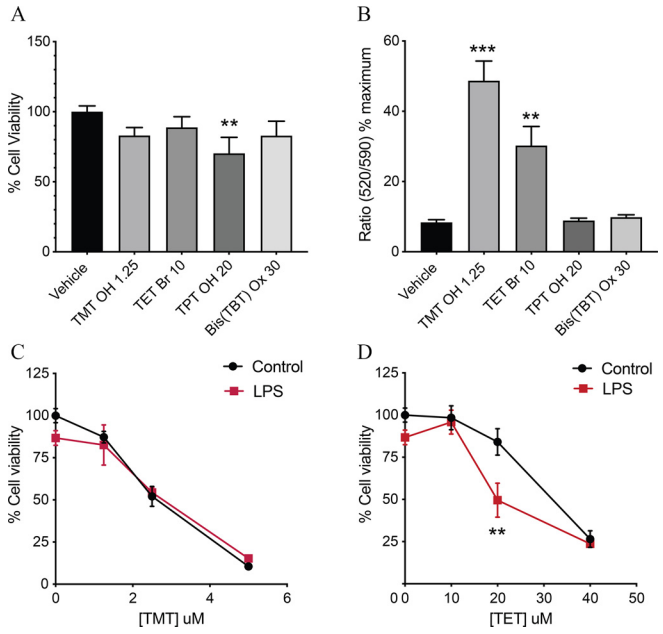

Figure 2. Cell viability and mitochondrial membrane permeability (MMP). (A) Cell viability of RAW 264.7 cells following 6-h exposure to vehicle (PBS), trimethyltin hydroxide (TMTOH; 1.25 μM), triethyltin bromide (TETBr; 10 μM), triphenyltin hydroxide (TPTOH; 20 μM) or Bis tributyltin oxide [Bis(TBT)Ox; 30 μM]. Data represent means ± SDs as percentages of controls ($n = 6$). (B) Estimates of mitochondrial stress using JC-10 assay. Data represent mean percentages of maximum response to antimycin ± SD ($n = 6$). (C,D) Cell viability following 6-h exposure to various doses of (C) TMTOH (0–5μM) or (D) TETBr (0–40μM) in nonprimed and LPS-primed cells (33 ng/mL, 3 h). Data were analyzed by one-way ANOVA followed by a Dunnett's test and represent means ± SDs ($n = 6$). The numerical data corresponding to this figure are shown in Excel Table S5. $^{****}p < 0.0001$; $^{***}p < 0.001$; $^{**}p < 0.01$; $^{*}p < 0.05$. Note: ANOVA, analysis of variance; LPS, lipopolysaccharide; PBS, phosphate buffered saline; SD, standard deviation.

comparisons tests. Bartlett's test was used for homogeneity of variance. ATP-linked respiration and maximum respiration were analyzed by a Kruskal-Wallis test followed by a Dunn's test. Significant p-values are listed as adjusted p-values where appropriate. All experiments were run with technical duplicates or triplicates, and we confirmed findings across at least two independent experiments. Group sample sizes are stated in the figure legends.

Results

Cell Viability and MMP

RAW 264.7 cell viability as assessed at 6-h exposure to TMTOH (1.25 μM = 0.226 μg/mL = 0.2 μgTMT/mL), TETBr (10 μM = 2.8 μg/mL = 2 μgTET/mL), or Bis-(TBT)Ox (30 μM = 17.8 μg/mL = 8.7 μg TBT/mL) was ≥75% (Figure 2A). The 30% lower cell viability seen with TPTOH (20 μM = 7.3 μg/mL = 4.7 μg TPT/mL), reached statistical significance ($p < 0.01$). MMP was examined at 6-h exposure and values were calculated relative to a maximum response to the positive control, antimycin, with a higher ratio indicating lower levels of MMP. With 6 h of exposure, TMTOH (1.25 μM) induced a disruption of ∼50% ($p < 0.001$) of maximum response and TETBr (10 μM) showed a disruption of ∼30% ($p < 0.01$) (Figure 2B). Similar MMP levels were seen with the addition of LPS for 3 h (vehicle 9 ± 0.6; TMT 57.4 ± 12.2; TET 40.1 ± 6.8). No differences were observed with TPTOH or Bis-(TBT)Ox. In an independent experiment, cell viability following different levels of TMTOH (Figure 2C) or TETBr (Figure 2D) was overall not significantly altered by LPS-priming; however, at 20 μM TET, cells primed with LPS showed ∼50% lower viability as compared with non-LPS-primed cells ($p < 0.01$).

TNFα Protein Release

To determine whether tri-organotin compounds induced a pro-inflammatory response, levels of TNFα and IL-1 protein released into the media were determined after 6 h of exposure. Cells exposed to TPTOH or Bis(TBT)Ox showed levels of TNFα similar to that observed with the PBS vehicle. Slightly higher protein levels (12%) were observed in cells exposed to TMTOH ($p = 0.002$) or TETBr ($p = 0.022$) as compared with controls (Figure 3A). LPS significantly elevated TNFα levels across all groups ($p < 0.0001$); however, in comparison to PBS, elevations in response to LPS exposure were ∼50% lower following subsequent exposure to TMTOH ($p < 0.0001$) or TETBr ($p < 0.0002$). In LPS-primed cells, TNFα was ∼50% higher in cells exposed to TPTOH ($p < 0.0001$). No difference was observed with Bis(TBT)Ox.

IL-1 Protein Release

NLRP3 inflammasome activation induces the cellular release of mature IL-1β (Martinon et al. 2002). As an initial evaluation, HEK-Blue IL-1R cells were used as an indicator of released bioactive IL-1 (IL-1α and IL-1β) from RAW 264.7 cells. A higher level of total IL-1 was observed with the positive control, within range of the maximum level of the assay. Levels following tri-organotin exposure were not significantly different from PBS exposure (Figure 3B). IL-1β ELISA was next used to determine the release of total IL-1β into the medium of RAW 264.7 cells. No increases were observed in non-LPS-primed cells exposed to the tri-organotins (Figure 3C) In LPS-primed cells, however, significant higher levels (∼2-fold) were observed with TMTOH ($p < 0.0001$) and TETBr ($p = 0.0262$), and a 10-times higher level with the NLRP3 activator, ATP ($p < 0.0001$) (Figure 3C). No elevations were observed with TPTOH or Bis(TBT)Ox.

In the absence of elevations in total IL-1β with TPTOH or Bis(TBT)Ox in LPS-primed cells, Western blots to discriminate between pro- (37 kD) and mature (17 kD) IL-1β protein were conducted for TMTOH and TETBr only. In RAW 264.7 cells, IL-1β was not observed in either the supernatant or lysate in the absence of LPS-priming (Figure 3D). With LPS-priming, triggering of NLRP3 inflammasome activation with the positive control, ATP, induced a release of mature IL-1β within 30 min. A secondary exposure to TMTOH or TETBr resulted in the release of low levels of IL-1β (Figure 3D). Pro-IL-1β was also detected in the lysate of LPS-primed cells exposed to TMTOH or TETBr (Figure 3D). Quantitation of protein band density across three gels and five independent samples demonstrated a ratio of released pro- (∼45%) or mature- (∼55%) IL-1β to total protein across exposures (Figure 3E). In primary murine BMDMs (Figure 3F), mature IL-1β release from LPS-primed cells was detected following exposure to ATP or tri-organotins.

ASC Speck Assembly

ASC speck formation has been effectively used as a readout for inflammasome activation (Stutz et al. 2013). Visualization of ASC speck formation was examined over 24 h by live-cell imaging of cerulean-tagged ASC aggregation in RAW 264.7-ASC cells (Figure 4A). Quantitation of ASC speck formation was conducted at 6 and 16 h (Figure 4B). In cells exposed to PBS, LPS, or ATP, a diffuse cytoplasmic fluorescence was observed. In LPS-primed cells, a 30-min exposure to ATP resulted in a dense coalesced staining pattern representative of aggregates, suggestive of NLRP3 inflammasome assembly. Non-LPS-primed cells exposed to TMTOH maintained a diffuse cerulean staining

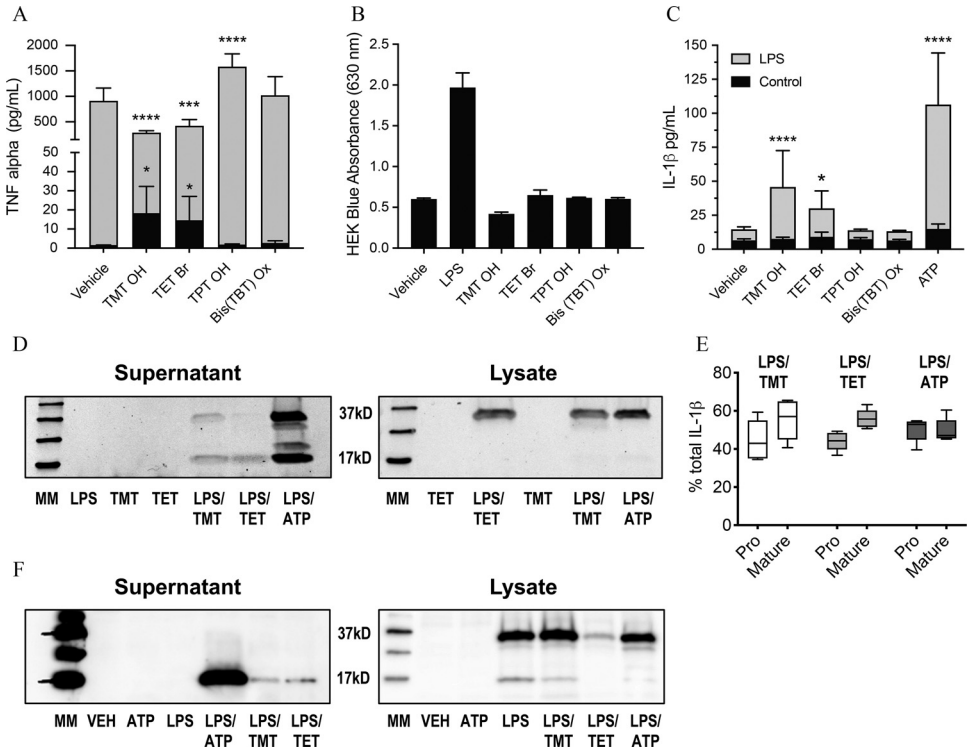

Figure 3. Protein levels for TNFα and IL-1. (A) TNFα protein levels determined by ELISA in nonprimed (black) and LPS-primed (gray, 33 ng/mL, 3 h) RAW 264.7 cells following 6-h exposure to vehicle (PBS), TMTOH (1.25 μM), TETBr (10 μM), TPTOH (20 μM) or Bis(TBT)Ox (30 μM) ($n=6$, nonprimed cells; $n=5$, TETBr or TPTOH). (B) Release of IL-1 protein as detected by HEK-Blue IL-1R cells following 6-h exposure to tri-organotins ($n=5$–6). (C) IL-1β protein levels as determined by ELISA in nonprimed (black) and LPS-primed (gray) RAW 264.7 cells following 6-h exposure to tri-organotins ($n=6$). Data represent means ± SDs. (D, E) IL-1β release upon exposure to TMT or TET in LPS-primed cells. (D) Representative Western blot of supernatant or lysate from RAW 264.7 cells for pro- (37kD) and mature (17kD) IL-1β and molecular weight marker (MM). (E) Quantitation of Western blot immunoreactive bands for pro- and mature IL-1β presented as the percentage of total IL-1β. Box plots represent median, first and third quartiles, and minimum and maximum values ($n=5$–6). Trim signal range for LPS+TMT (pro-, 100–300; mature, 250–400), LPS+TET (pro-, 9–30; mature, 17–50), ATP (pro-, 2,000; mature, 4,000). (F) Representative Western blot of supernatant or lysate from BMDM cells for pro- and mature IL-1β. The numerical data corresponding to this figure are shown in Excel Table S6. $^{****}p<0.0001$; $^{***}p<0.001$; $^{*}p<0.05$ as compared with matched vehicle (PBS) control. Note: ATP, adenosine triphosphate; Bis(TBT)Ox, Bis tributyltin oxide; BMDM, bone marrow-derived macrophage; ELISA, enzyme-linked immunosorbent assay; IL, interleukin; LPS, lipopolysaccharide; PBS, phosphate buffered saline; SD, standard deviation; TET, triethyltin; TETBr, triethyltin bromide; TMT, trimethyltin; TMTOH, trimethyltin hydroxide; TNF, tumor necrosis factor; TPTOH, triphenyltin hydroxide.

pattern that did not change significantly over time. This differed for TETBr, where the compound alone was sufficient to induce a minor level of aggregate assembly at 6 h ($p=0.003$), which increased by 16 h ($p<0.0001$). In LPS-primed cells, ASC speck formation was significantly higher with TMTOH (6 h $p=0.0049$; 16 h $p<0.0001$) and TETBr ($p=0.006$; 16 h $p<0.0001$) as compared with LPS-controls. ASC speck assembly was not observed for TPTOH (Figure S2). Because extracellular ATP can serve as an autocrine/paracrine trigger for NLRP3 activation via activation of P2XR, cells were treated with the ATP-hydrolytic enzyme apyrase. The higher level of ASC speck formation observed with LPS priming was partially inhibited with apyrase, suggesting a contribution from extracellular ATP. For TMTOH, ASC speck formation was effectively inhibited by apyrase at 6 and 16 h. For TETBr, the significantly higher level of ASC speck formation at 16 h in nonprimed and LPS-primed cells was observed with apyrase ($p<0.01$), suggesting a direct triggering effect in addition to that of extracellular ATP.

Caspase-1 Activation

The assembly of the NLRP3 inflammasome activates caspase-1 and mediates processing of IL-1β Martinon et al. 2002). Given the subtle differences observed for ASC speck formation in LPS-primed cells in response to TETBr as early as 6 h, we examined the concurrent cell expression of active caspase-1, using a caspase-1 substrate, FAM-FLICA, which yields fluorescence upon cleavage (Figure 4C–F). Single cells were examined on a FAM-FLICA caspase-1 plot to determine the population shift of positive cells as represented in contour plots (Figure 4C), histogram distribution patterns (Figure 4D), and associated quantitation of caspase-1 (Figure 4E) and PI (Figure 4F). There was no indication of active caspase-1^+ cells in PBS- or LPS-dosed cells. In non-LPS-primed cells, TETBr exposure resulted in slightly higher ($p<0.05$). caspase-1^+ cells ($\sim 8\%$) mean fluorescence intensity (MFI) (2-fold). Similar higher levels were observed for TMTOH; however, this failed to reach statistical significance. In LPS-primed cells, percentage caspase-1^+ cells and MFI were significantly higher with ATP exposure ($p<0.01$). LPS-primed cells exposed to TMTOH showed a higher number ($\sim 12\%$) of caspase-1^+ cells ($p<0.01$) and 2-MFI (2-fold; $p<0.05$) as compared with LPS-primed+vehicle cells. Levels with TETBr were not significantly different from comparable vehicle controls. No differences were observed in LPS-primed cells exposed to TETBr as compared with LPS-primed+vehicle cells. Inflammasome activation can lead to pyroptotic cell lysis detected by PI staining and estimations of cell swelling (Figure 4F). With evidence of inflammasome activation by 6 h, cell size (forward-scattered light) was $\sim 10\%$ larger across all groups, as compared with PBS, which did not reach statistical significance. Percentage PI cell staining, excluding cellular

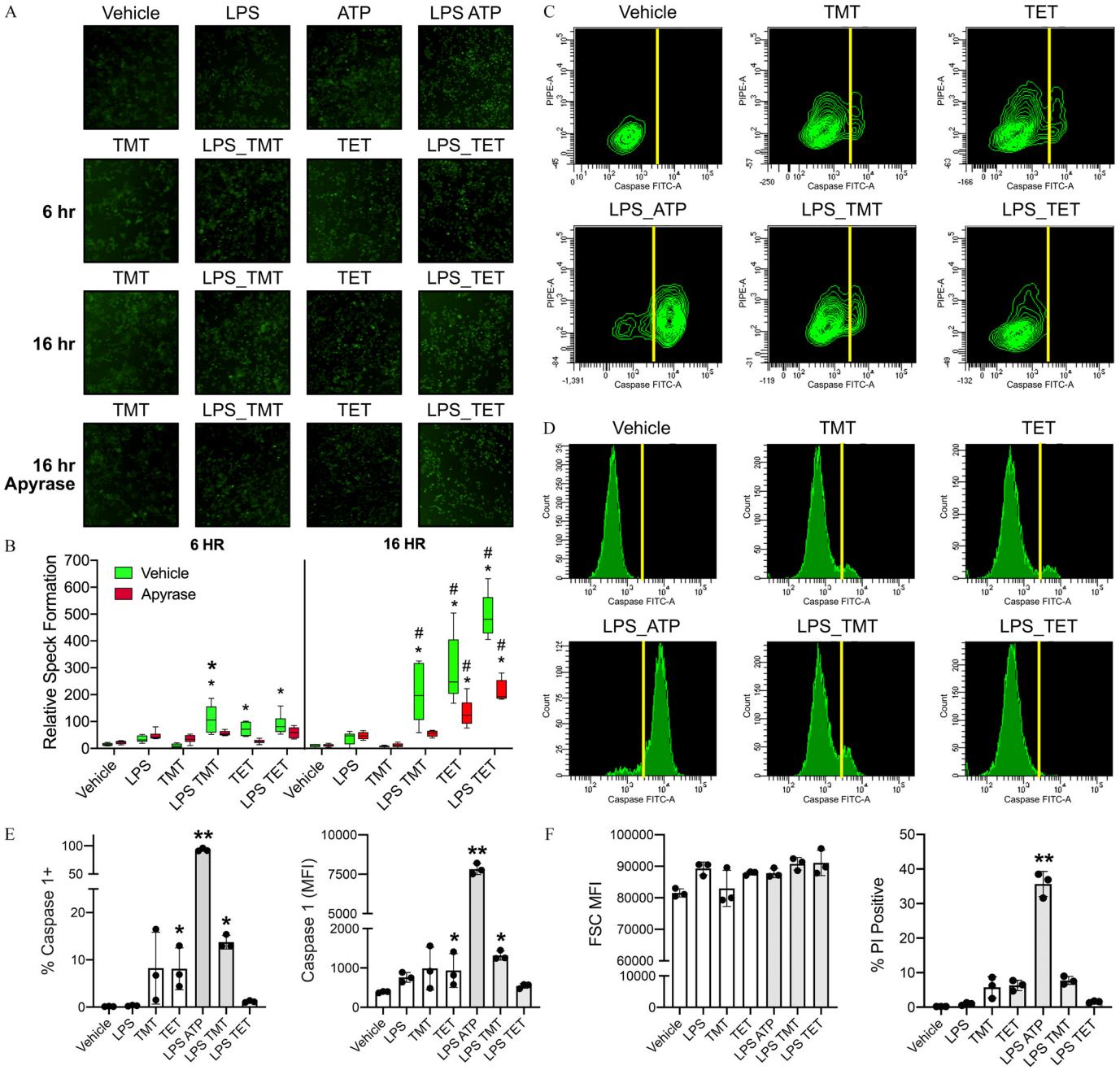

Figure 4. NLRP3 inflammasome activation. (A) Representative images of RAW 264.7 ASC speck cells and inflammasome activation as indicated by condensed fluorescent aggregates in cells exposed to vehicle (PBS; 19 h), LPS (33 ng/mL; 19 h), ATP (5 nM; 30 m) or LPS+ATP; LPS-primed (3 h) and non-LPS-primed cells exposed to TMTOH (1.25 μM; TMT) or TETBr (10 μM; TET) for 6 or 16 h or with apyrase coexposure for 16 h. Images were captured using a 20-magnification objective on an IncuCyte S3 live-cell analysis system and IncuCyte ZOOM 2015A software. (B) Quantitation of relative ASC speck aggregation in nonprimed and LPS-primed cells in the absence or presence of apyrase with exposure to TMTOH or TETBr. Box plots represent median, first and third quartiles, and minimum and maximum values ($n = 6$) analyzed by two-way ANOVA followed by Tukey's multiple comparisons tests. $^{*}p < 0.01$ compared with LPS-matched control; $\#p < 0.01$ compared with matched group at 6 h. (C, D) Representative (C) contour plots and (D) histograms of flow cytometry for active caspase-1 at 6 h (see Figure S1 for information on gating). (E) Flow cytometric analysis of percentage active caspase-1^{+} cells and mean fluorescence intensity (MFI). (F) Cell size (forward-scattered light) and percentage cell death (PI^{+}) with tri-organotin exposure. Data were analyzed by one-way ANOVA and graphs represent individual values, means ± SDs ($n = 3$). The numerical data corresponding to this figure are shown in Excel Table S7. $^{*}p < 0.05$, $^{**}p < 0.01$. Note: ANOVA, analysis of variance; ASC, apoptosis-associated speck-like protein containing a caspase recruitment domain; ATP, adenosine triphosphate; FITC, fluorescein isothiocyanate; FSC, forward scatter channel; LPS, lipopolysaccharide; MFI, mean fluorescence intensity; NLRP3, nucleotide-binding oligomerization domain-like receptor family, pyrin domain-containing receptor 3; PBS, phosphate buffered saline; PI, propidium iodide; PIPE-A, propidium iodide detected in the PE-A channel; SD, standard deviation; TET, triethyltin; TETBr, triethyltin bromide; TMT, trimethyltin; TMTOH, trimethyltin hydroxide.

debris was <10% with exposure to LPS, TMTOH, TETBr, or LPS+TMTOH. No difference was observed with LPS+TETBr. For the LPS+ATP positive control, this was significantly greater at ~35% ($p < 0.001$).

Nitrite Production and Cellular and mtROS Levels in Cells Exposed to Tri-Organotins

At 6 h, nitrite production remained low but was ~20% higher in cells exposed to TETBr, as compared with PBS exposure

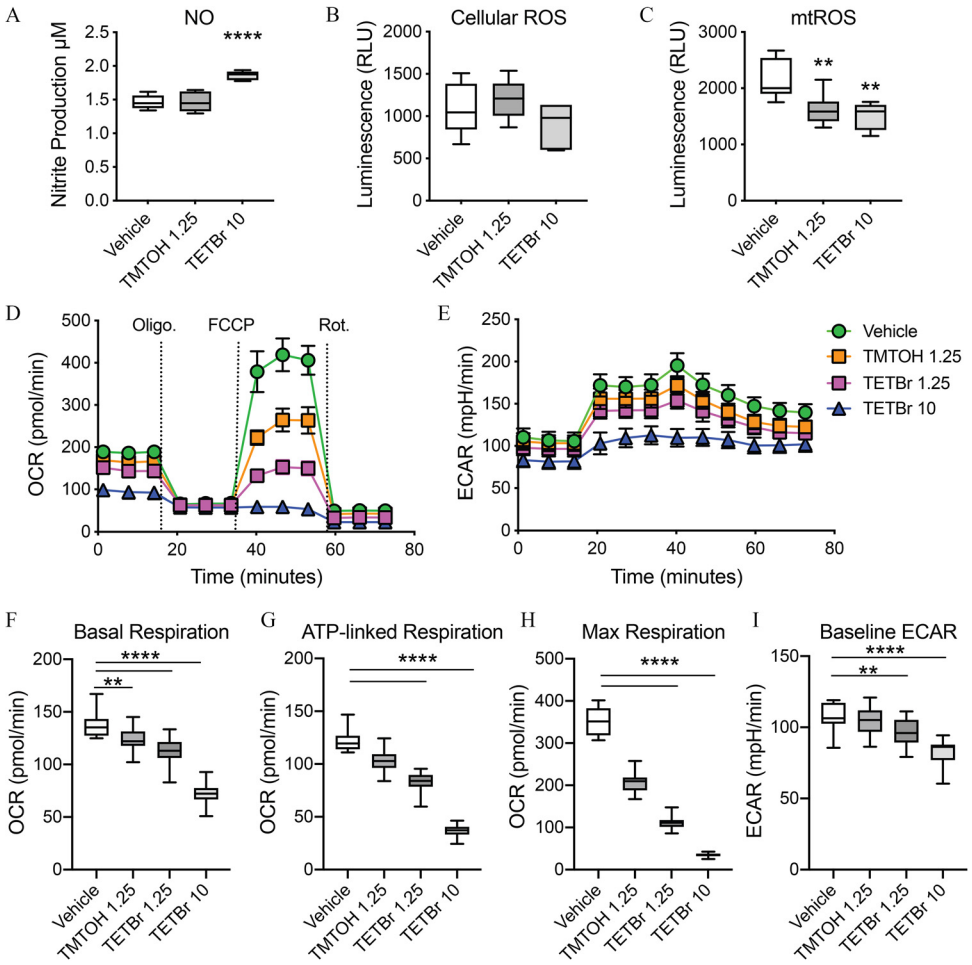

Figure 5. Nitric oxide (NO), reactive oxygen species (ROS), and mitochondrial bioenergetics. (A) Nitrite accumulation from RAW 264.7 cells following 6-h exposure to vehicle (PBS), TMTOH (1.25 µM), or TETBr (10 µM) (determined by Griess assay) ($n = 6$). (B,C) ELISA for DMPO (in triplicate) as indicator for (B) cellular ROS and (C) mitochondrial ROS (mtROS) ($n = 9$). Data were analyzed by one-way ANOVA followed by Dunnett's tests. (D) Representative mitochondrial bioenergetics profile of RAW 264.7 cells exposed to vehicle (PBS), TMTOH (1.25 µM), or TETBr (1.25 or 10 µM) for 6 h. After signal stabilization (three measures) cells were sequentially exposed to the mitochondrial stressors: oligomycin (Oligo), FCCP, and rotenone (Rot) and the oxygen consumption rate (OCR) quantified. (E) Representative glycolytic profile [extracellular acidification rate (ECAR)] of exposed cells under the bioenergetic paradigm. (F) Basal respiration, (G) ATP-linked respiration, (H) maximum respiration, and (I) basal glycolytic rate (i.e., ECAR) ($n = 15$). Data were analyzed by a one-way ANOVA followed by Dunnett's tests for basal respiration and basal glycolytic rate or by a Kruskal-Wallis test followed by a Dunn's test for ATP-linked and maximum respiration. Data represent means ± SDs (control: $n = 10$; organotins: $n = 24$). Box plots represent median, first and third quartiles, and minimum and maximum values. The numerical data corresponding to this figure are shown in Excel Table S8. $^{**}p < 0.01$; $^{****}p < 0.0001$. Note: ANOVA, analysis of variance; ATP, adenosine triphosphate; DMPO, 5,5-dimethyl-1-pyrroline *N*-oxide; ECAR, extracellular acidification rate; ELISA, enzyme-linked immunosorbent assay; FCCP, carbonyl cyanide-4-(trifluoromethoxy)phenylhydrazone; OCR, oxygen consumption rate; PBS, phosphate buffered saline; RLU, relative light unit; SD, standard deviation; TETBr, triethyltin bromide; TMTOH, trimethyltin hydroxide.

($p < 0.0001$). No increase was observed with TMTOH (Figure 5A). To determine whether tri-organotins increased ROS, mtROS and cellular ROS levels were determined. Immuno-spin trapping analysis by DMPO ELISA showed no elevation of free radical-derived protein–nitrone adducts in whole-cell homogenate (Figure 5B). Significantly overall lower levels were observed in mtROS levels ($F_{(2,20)} = 12.01, p = 0.0004$) of ~25% for TMTOH ($p = 0.001$) and TETBr ($p = 0.001$), relative to PBS (Figure 5C).

Mitochondrial Bioenergetics

Given that we did not observe elevations in ROS levels by tri-organotins, we examined potential alterations in mitochondrial bioenergetics induced by TMTOH or TETBr. In control cells, OCR and extracellular acidification rate (ECAR) profiles—surrogate measures for oxidative phosphorylation and glycolysis, respectively—demonstrated expected response patterns for basal respiration and following FCCP and rotenone stressors (Figure 5D,E). Exposure levels of the tri-organotins were initially selected based on equivalent cell viability over 24 h; however, given the severity of the mitochondrial respiratory effects of TETBr (10 µM), the response was also examined at 1.25 µM. Tri-organotin exposure lowered basal respiration, relative to PBS exposure ($F_{(3,78)} = 144.3$, $p < 0.0001$; Figure 5F). Levels were lower with TMTOH (~15%; $p = 0.0014$) or TETBr (10 µM ~40%; 1.25 µM ~20%; $p < 0.0001$). Kruskal-Wallis tests indicated significant differences in ATP-linked respiration (72.15;$p < 0.0001$; Figure 5G) and maximum respiration (74.77;$p < 0.0001$; Figure 5H). Significant differences in ATP-linked respiration were not observed for TMTOH yet were lower for TETBr (10 µM, 70%; 1.25 µM, 30%; $p < 0.0001$). Maximum respiration was not significantly different for TMTOH ($p = 0.17$) but was significantly lower for TETBr (10 µM, 90%; 1.25 µM, 70%; $p < 0.0001$). Simultaneous measurements of ECAR (Figure 5I) indicated a significant effect of tri-organotin exposure ($F_{(3,78)} = 29.89$, $p < 0.0001$) with lower levels with TETBr (10 µM, ~30%; $p < 0.0001$ and 1.25 µM, ~15%; $p < 0.01$). Cell

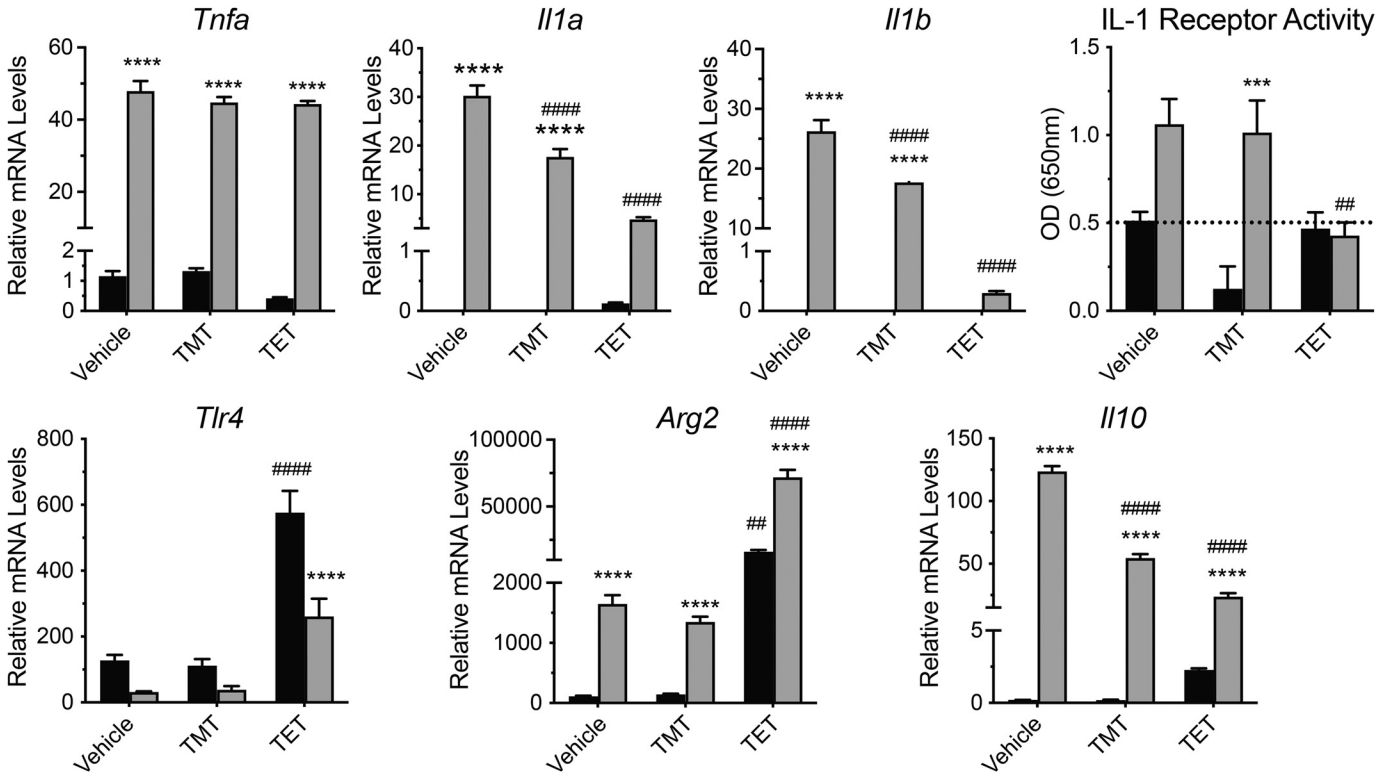

Figure 6. Real-time qPCR for cytokine mRNA levels in RAW 264.7 cells in response to LPS following exposure to TMTOH (TMT) or TETBr (TET). mRNA levels for *Tnfa*, *Il1a*, *Ilb*, *Tlr4*, *Arg2*, *Il10*, *Gapdh*, and IL-1 receptor activity (HEK-Blue IL-1R cells) in cells exposed to vehicle (PBS), TETBr (1.25 μM), or TMTOH (10 μM) for 6 h followed by the addition of either vehicle (PBS; dark bars) or LPS (33 ng/mL; light bars) for 3 h ($n = 6$). The dashed line indicates the average response of control cells for reference. Relative mRNA amounts were calculated using a normalized standard curve and expressed as ratios of target gene to *Gapdh*. Data were analyzed by a two-way ANOVA for each end point followed by Dunnett's multiple comparisons tests. The numerical data corresponding to this figure are shown in Excel Table S9. $^{****}p < 0.0001$; $^{***}p < 0.001$; $^{*}p < 0.05$ compared with matched non-LPS cells within each exposure group. $\#\#\#\#p < 0.0001$; $\#\#p < 0.01$ compared with matched vehicle (PBS) or vehicle+LPS. Note: ANOVA, analysis of variance; IL, interleukin; LPS, lipopolysaccharide; OD, optical density; PBS, phosphate buffered saline; qPCR, quantitative polymerase chain reaction; TET, triethyltin; TETBr, triethyltin bromide; TMT, trimethyltin; TMTOH, trimethyltin hydroxide; TNF, tumor necrosis factor.

density was visually confirmed as equivalent across samples prior to and immediately following the assay.

LPS- and LPS/ATP-Stimulated Cytokine Release

We evaluated whether the exposure altered the ability of RAW 264.7 cells to respond to LPS (Figure 6). No differences were observed with tri-organotin exposure alone, compared with controls. LPS significantly elevated *Tnfa* ($p < 0.0001$) in all groups compared with vehicle, with no differences observed due to tri-organotin exposure. *Il1a* and *Il1b* were elevated by LPS in all groups ($p < 0.0001$); however, the level of induction was significantly attenuated in cells exposed to TMTOH ($\sim 30\%$) or TETBr ($\sim 60\%$) ($p < 0.0001$). IL-1 receptor activity, as determined by HEK-Blue IL-1R cells, was higher in cells exposed to PBS or TMTOH ($p < 0.001$) and subsequently treated with LPS. This was not observed in cells exposed to TETBr. *Tlr4* was significantly elevated with TETBr (3-fold; $p < 0.0001$) and the relative lower levels observed with LPS-priming were similar across groups. *Arg2* was elevated with TETBr (~ 2-fold; $p < 0.001$) and in all groups with LPS-priming ($p < 0.0001$). *Il10* was slightly (2-fold) elevated with TETBr and with LPS priming; however, the elevation in LPS-primed cells was significantly less ($\sim 50\%$) in TMTOH and TETBr exposed cells as compared with PBS ($p < 0.0001$).

ASC Speck Formation and LPS/ATP-Stimulated Cytokine Release at Lower Tri-Organotin Levels

To examine related alterations due to a lower exposure level, RAW 264.7 cells were examined for ASC speck formation as triggered by either TETBr (1.0 μM = 0.2 μg/mL) or TMTOH exposure (0.06 μM = 0.01 μg/mL), showing an induction (Figure 7A). To determine whether the lower dose levels would alter the normal inflammasome induction, the cells were exposed for 18 h to either TETBr (1.0 μM = 0.2 μg/mL) or TMTOH (0.05 μM = 0.009 μg/mL) prior to inflammasome activation [LPS priming (33 ng/mL; 3 h) followed by a secondary ATP trigger (5 mM; 30 min)]. Under these conditions, no alterations were observed in *Tnfa* levels, whereas *Il1a* and *Il1b* levels were lower (<75%) with prior exposure to TMT ($p < 0.001$) or TET ($p < 0.001$) (Figure 7).

miRNA Expression Profile in LPS-Primed Cells Exposed to Tri-Organotins

Differences were observed between TMTOH and TETBr that may have represented a difference in severity or underlying signaling pathways. miRNAs serve as major players in the regulation of NLRP3 inflammasome activation at both the priming and secondary trigger steps (O'Neill et al. 2011; Rebane and Akdis 2013; Zamani et al. 2020). To interrogate for underlying cellular changes induced by tri-organotins that might account for differences observed between the two, murine BMDMs were used to generate miRNA (Figure 8) and mRNA profiles (Figure 9). For miRNAs, distribution patterns across the different exposure groups suggested a robust distribution shift with TETBr in LPS-primed cells, compared with LPS alone (Figure 8A,B). The profile showed differences in 150 miRNAs [81 higher; 69 lower] for TETBr and only 17 miRNAs [12 higher; 5 lower] for TMTOH (Figure 8C). Of

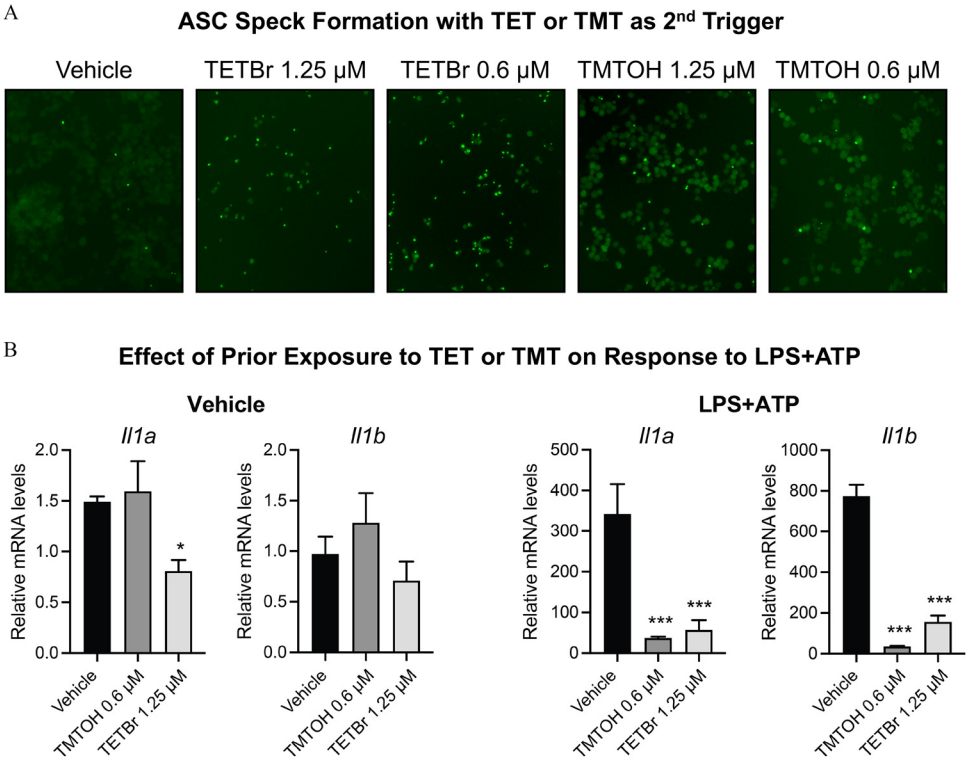

Figure 7. ASC speck formation and mRNA levels for *Il1a* and *Il1b*. (A) Representative images of ASC speck formation in LPS-primed RAW 264.7 cells following 16-h exposure to vehicle (PBS, 19 ± 12), TETBr (1.25 μM, 319 ± 112; 0.6 μM, 297 ± 152) or TMTOH (1.25 μM, 181 ± 62; 0.6 μM, 53 ± 3). Inset numbers represent quantitation of ASC specks within the ROI. Images are captures under a 20-manification objective. (B) mRNA levels for *Il1a* and *Il1b* in RAW 264.7 cells exposed to vehicle (PBS), TMTOH (0.05 μM), or TETBr (1.0 μM) for 18 h followed by LPS (33 ng/mL; 3 h) then ATP (5 mM; 30 min) ($n = 4$). Cell viability estimates at 21 h of the tri-organotin with LPS were $\sim 95 \pm 7\%$ for TMTOH and $90 \pm 5\%$ for TETBr, relative to control ($n = 4$). mRNA levels were normalized to *Gapdh*. Data were analyzed by a two-way ANOVA for each end point followed by Dunnett's multiple comparisons tests. The numerical data corresponding to this figure are shown in Excel Table S10. $^{*}p < 0.01$; $^{***}p < 0.0001$ compared with vehicle of respective vehicle (non-LPS) or LPS+ATP group. Note: ANOVA, analysis of variance; ASC, apoptosis-associated speck-like protein containing a caspase recruitment domain; ATP, adenosine triphosphate; LPS, lipopolysaccharide; PBS, phosphate buffered saline; ROI, region of interest; TETBr, triethyltin bromide; TMTOH, trimethyltin hydroxide.

these, 146 miRNAs [78 higher; 68 lower] were unique to TETBr. Thirteen [9 higher; 4 lower] were unique to TMTOH. Of the significantly altered miRNAs, 4 were shared between the two tri-organotins with 3 higher (*miR-6909-5p, miR-7044-5p, miR-7686-5p*) and one lower *(miR-151-3p*) (Figure 8B; Excel Table S2).

Targeted examination was next conducted on several miRNAs previously identified as regulators of NLRP3 inflammasome activation (Boxberger et al. 2019; Tezcan et al. 2019; Zamani et al. 2020). Of the 68 miRNAs found lower only with TETBr, those previously reported as related to NLRP3 inflammasome activation included the TLR4 receptor expression inhibitor, *miR-146a* (Bhatt et al. 2016; Schnitger et al. 2011) and the *Nlrp3* inhibitors *miR-7* (Zhou et al. 2016), *miR-17-5p* (Chen et al. 2018), and *miR-22* (Chen et al. 2016; Huang et al. 2017). Those associated with multiple mechanisms to regulate inflammasome activation included *miR-23a* (Pan et al. 2018), *miR-23b* (Zhu et al. 2012), *miR-7* and *miR-30d-5p* (Zhou et al. 2016), *miR-30d-5p* (Liu et al. 2014), *miR-146a-5p* (Zhang et al. 2018), and *miR-711* (Boursereau et al. 2018). Of mitochondrial-related miRNAs associated with apoptosis, cell proliferation and differentiation (Barrey et al. 2011; Kren et al. 2009), and mitochondrial dysfunction (Bian et al. 2010), *miR-140-3p*, *miR-320*, *miR-26a-1*, *miR-677*, *miR-125a-5p*, were lower and *miR-671* and *miR-705* higher with TETBr exposure.

Gene Expression Profiles

miRNAs generally target more than one gene in a signaling pathway. Thus, to gain a better understanding of the target genes associated with the miRNAs altered by each tri-organotin, mRNA expression array profiles were examined (Figure 9). A predominant shift was observed with TETBr that was less with TMTOH (Figure 9A). When we examined targets for *miR-151-3p,* which was lower with both tri-organotins, 416 targets predicted by the TargetScan program were represented in the mRNA array. Functional analysis was performed on the up-regulated mRNA targets and the results indicated cyclic adenosine monophosphate (cAMP)-mediated signaling and AMP-activated protein kinase (AMPK) signaling to be the top enriched pathways (Figure 9C, Table S1). Three miRNAs (*miR-6909-5p*, *miR-7044-5p*, *miR-7686-5p*) were found to be expressed at a higher level with both tri-organotins. We then applied a functional analysis of the mRNA expression data, focusing on down-regulated mRNA targets of these miRNAs. Wnt beta-catenin signaling, retinoic acid receptor activation, apoptosis signaling, signal transducer and activator of transcription 3 (STAT3) pathway, as well as IL-22, IL-12, and IL-10 signaling, were among the top enriched pathways (Figure 9D; Excel Table S3).

To better understand these four miRNAs' potential RNA activation function, we performed additional analyses to identify potential miRNAs' binding sites in the 5′-untranslated region of mRNAs. From target mRNAs predicted by miRWalk and miRDB programs, we identified 11 potential targets for commonly down-regulated miRNA (*miR-151-3P*), with 8 positively correlated with *miR-151-3P*. However, no significantly enriched pathways were identified. Of the 58 potential targets for commonly up-regulated miRNAs (*miR-7686-5P*, *miR-7044-5P*, and

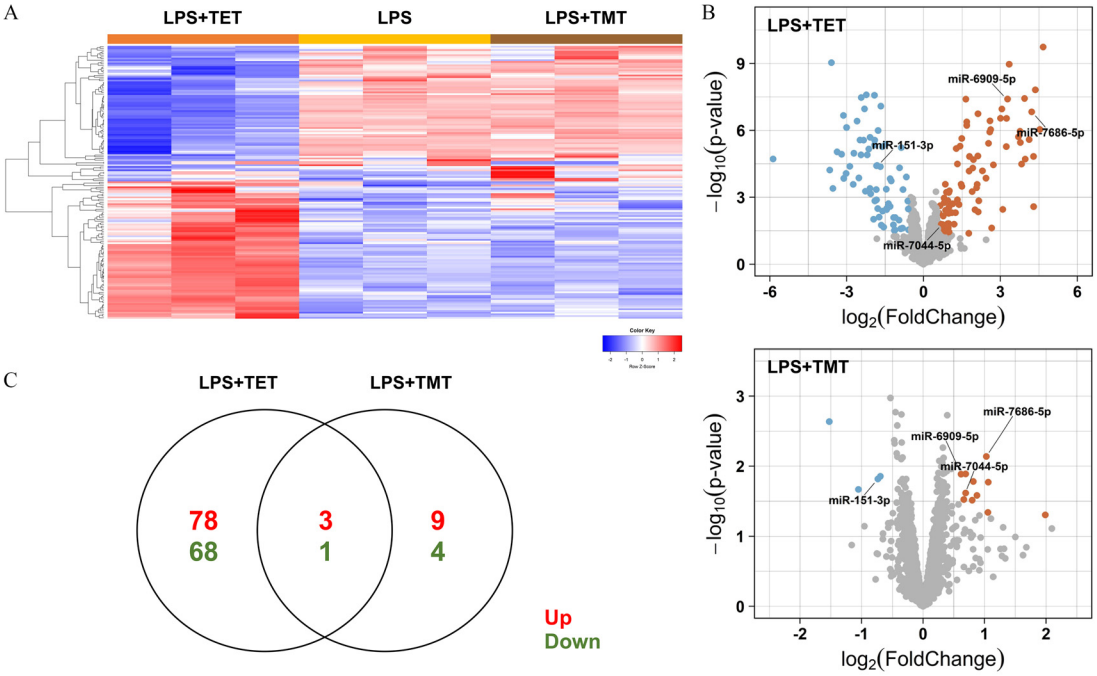

Figure 8. miRNA expression in BMDM exposed to TMTOH or TETBr. (A) Heatmap showing the differentially expressed miRNAs in LPS-primed cells upon 6-h exposure to TMTOH (1.25 μM) or TETBr (10 μM) as compared with LPS-primed cells exposed to vehicle (PBS) (B) Volcano plots of differentially expressed miRNA in LPS-primed cells following the second exposure to TMTOH or TETBr with four common miRNAs labeled (*miR-6909-5p*, *miR-7044-5p*, *miR-7686-5p*, and *miR-151-3p*). (C) Venn diagram representing distinct and common differentially expressed miRNAs in both LPS-primed TMTOH- or TETBr-exposed cells compared with LPS-primed cells exposed to vehicle (PBS). Three biological replicates for each group were included in the analysis. The numerical data corresponding to (C) are shown in Excel Table S2. Note: BMDM, bone marrow-derived macrophage; LPS, lipopolysaccharide; miRNA, microRNA; PBS, phosphate buffered saline; TET, triethyltin; TETBr, triethyltin bromide; TMT, trimethyltin; TMTOH, trimethyltin hydroxide.

miR-6909-5P), 47 positively correlated with these up-regulated miRNAs. The fibroblast growth factor signaling pathway (FGF12 and FGF7) was found to be significantly enriched (Table S2). When we applied a functional enrichment analysis on the differentially expressed mRNAs, a differential pattern of pathways was observed between TETBr and TMTOH LPS-primed cells (Excel Table S4). The top enriched canonical pathways were related to apoptosis (such as unfolded protein response and p53 signaling) or cell survival (such as hypoxia and other endoplasmic reticulum-stress related pathways), and senescence.

Real-Time qPCR mRNA Levels for P2rx7, P2rx4, and A20/Tnfaip3

Given the differential effect of apyrase on ASC speck formation observed in LPS-primed RAW 264.7 cells, the down-regulation of several miRNAs that target P2rx7 (*miR-22-3p*, *miR-125a-3p*, *miR-125a-5p*, and *miR-146a-5p*), and the up-regulation in P2rx7 (44.66 fold-change in LPS+TETBr–exposed BMDMs, we examined levels of *P2rx7* and *P2rx7* in BMDMs by real-time qPCR. In non-LPS-primed cells, *P2rx7* levels with tri-organotin exposure were slightly lower but failed to reach statistical significance. As compared with non-LPS-primed controls, LPS-primed cells showed lower *P2rx7* levels ($p = 0.007$). With LPS-priming, *P2rx7* levels were significantly lower with TMTOH ($p < 0.005$) and higher with TETBr (compared with PBS: $p = 0.004$; to non-LPS-primed TETBr: $p = 0.005$) (Figure 10), which could reflect sensitization to extracellular ATP. In non-LPS-primed cells, *P2rx4* was not altered with TMTOH and lower with TETBr ($p < 0.003$). In LPS-primed cells exposed to TETBr, *P2rx4* levels were slightly lower than LPS+PBS but failed to reach statistical significance. Levels of *A20*, a target gene of let-7, *miR-125a*, *miR-125b*, were significantly higher in LPS-primed cells exposed to TETBr ($p < 0.0001$) as compared with vehicle controls (Figure 10).

Discussion

Inflammation can be viewed as a complicated series of local immune responses to deal with a threat to the microenvironment. The appropriate regulation of the initial cellular response to tissue damage facilitates recovery, whereas uncontrolled neuroinflammation can induce secondary injury. Although environmental agents can directly or indirectly, as a result of cell injury, induce a pro-inflammatory response, they may also show the ability to modify a normal response of immune cells. The fact that this may occur in the absence of a pro-inflammatory induction raises a concern in addressing how exposures might contribute across a broad spectrum of human health or with various comorbidities. The interactive role of mitochondria with innate immune responses, including NLRP3 inflammasome activation, offers a cellular mechanism by which factors known to alter mitochondrial function may initiate or dysregulate an immune response. In examining a set of tri-organotin compounds that have been previously demonstrated to induce a spectrum of effects on oxidative phosphorylation and to alter aspects of immune cell function, we demonstrated that the two known neurotoxicants, TETBr and TMTOH, showed evidence of inducing IL-1β release in LPS-primed macrophages. Although the levels were low, the relative levels observed were within ranges previously reported for NLRP3 inflammasome activation in macrophages following oxidized low-density lipoprotein (Sheedy et al. 2013) or silica (Dostert et al. 2008). Prior studies have suggested that ROS activation is an essential element for NLRP3 inflammasome activation (Abais et al. 2015); however, we observed no induction of cellular or mtROS yet, alterations in mitochondrial bioenergetics. Further examination of alterations related to IL-1β release in

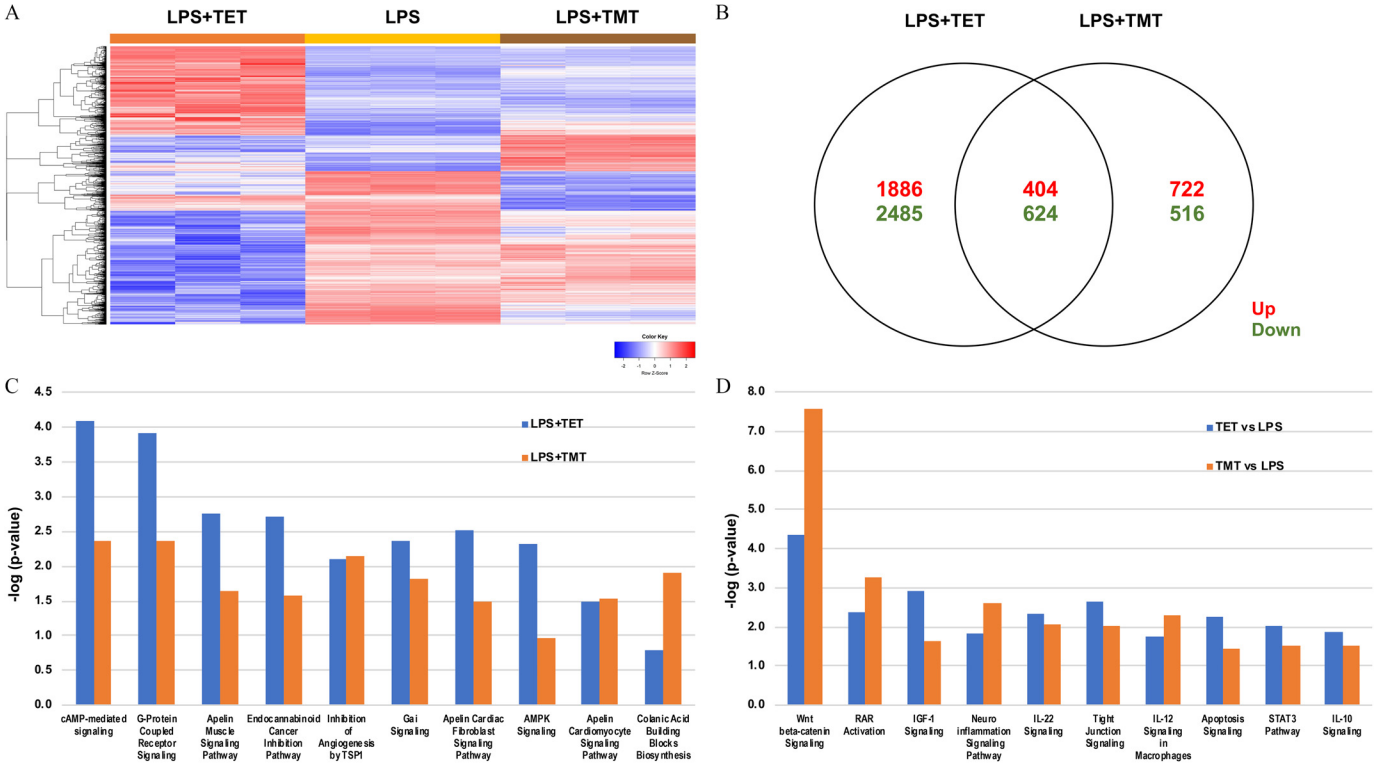

Figure 9. Transcriptomic analysis of gene expression changes in BMDM cells exposed to TMTOH or TETBr. Three biological replicates were identical to samples analyzed for mRNA expression. (A) Representative heatmap of the differentially expressed mRNAs in LPS-primed cells upon 6-h exposure to TMTOH (1.25 μM) or TETBr (10 μM) as compared with LPS-primed cells exposed to vehicle (PBS). (B) Venn diagram of the distinct and common differentially expressed genes under each exposure condition as compared with LPS-primed cells. (C) Functional analysis of up-regulated mRNA targets for *miR-151-3p*, which was lower with both tri-organotins exposed cells relative to LPS-primed cells. (D) Functional analysis of down-regulated mRNA targets for miRNAs [*miR-6909-5p*, *miR-7044-5p*, *miR-7686-5p*] that were higher in both LPS-primed TMTOH- and LPS-primed TETBr-exposed cells as compared with LPS-primed cells. The numerical data corresponding to this figure are shown in Table S1 and Excel Table S3). Note: AMPK, adenosine monophosphate-activated protein kinase; BMDM, bone marrow-derived macrophage; cAMP, cyclic adenosine monophosphate; G, guanine nucleotide; IGF1, insulin-like growth factor 1; IL, interleukin; LPS, lipopolysaccharide; miRNA, microRNA; PBS, phosphate buffered saline; RAR, retinoic acid receptor; STAT3, signal transducer and activator of transcription 3; TET, triethyltin; TETBr, triethyltin bromide; TMT, trimethyltin; TMTOH, trimethyltin hydroxide; TSP1, Thrombospondin 1.

LPS-primed cells identified differential miRNA and mRNA expression profiles with TMTOH or TETBr exposure that may contribute to understanding the cellular response to such insults and how they may manifest as immune cell dysregulation.

The field of immunometabolism emphasizes the importance of mitochondria in immune signaling (Lynch 2020; O'Neill et al. 2016; West 2017), with several studies demonstrating metabolic reprograming of macrophages to meet energy demands when responding to stimuli. In macrophages, a significant decrease in oxidative phosphorylation can reflect damage to mitochondria and diminished cellular function, but it can also indicate elevated glycolytic rate (Ganeshan and Chawla 2014) and underlie the metabolic shift observed with a pro-inflammatory response (Sanman et al. 2016). Although early work suggested that mitochondrial inhibition would be greater with TPT or TBT (Powers and Beavis 1991), we found that TETBr and TMTOH lowered

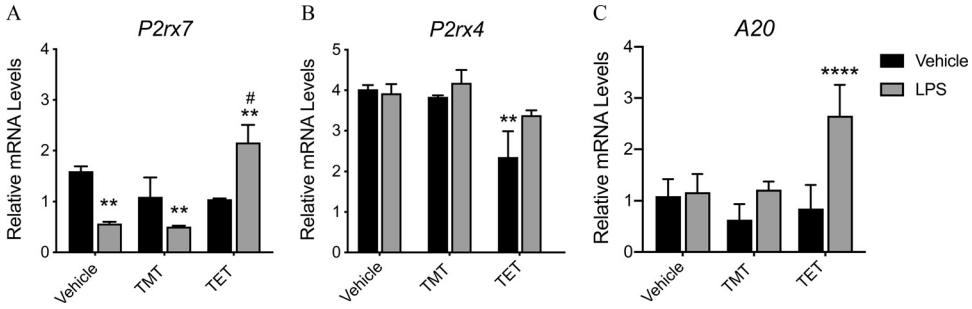

Figure 10. Real-time qPCR of (A) *P2rx7*, (B) *P2rx4*, and (C) *A20* levels in BMDM exposed to TMTOH or TETBr. mRNA levels were quantified by real-time qPCR (TaqMan) in BMDM following exposure to vehicle (PBS) or LPS for 3 h followed by the addition of vehicle (PBS), TMTOH (1.25 μM; TMT), or TETBr (10 μM; TET) for 6 h. Relative mRNA amounts were calculated using a normalized standard curve and expressed as ratios of target gene to *Gapdh*. Data were analyzed by a two-way ANOVA for each end point followed by a Tukey's test for multiple comparisons. Data represent mean relative mRNA ± SDs ($n = 6$). See Figure S4 for BMDM cell morphology. The numerical data corresponding to this figure are shown in Excel Table S11. $^{****}p < 0.0001$; $^{**}p < 0.01$ compared with non-LPS-primed cells exposed to vehicle (PBS) within each exposure group. $\#p < 0.01$ compared with LPS-primed cells+vehicle. Note: ANOVA, analysis of variance; BMDM, bone marrow-derived macrophage; LPS, lipopolysaccharide; PBS, phosphate buffered saline; qPCR, quantitative polymerase chain reaction; SD, standard deviation; TET, triethyltin; TETBr, triethyltin bromide; TMT, trimethyltin; TMTOH, trimethyltin hydroxide.

mitochondrial basal respiration and ECAR and stimulated IL-1β release in LPS-primed macrophages. As related to overall toxicity of the trialkyltin compounds, this would agree with the highest level of toxicity observed with the lower homologs, TMT and TET (Mushak et al. 1982; Snoeij et al. 1987) but would be in contrast to the previous severity ranking for oxidative phosphorylation (Powers and Beavis 1991). Mushak et al. (1982) reported that, regardless of the toxicity across tri-organotins, all showed significant levels in organs; however, detectable levels in the blood were observed only for TMT and TET. Evidence of immunotoxicity suggested a similar mode of action and potency for TBT and TPT (EFSA 2004); however, given the difference in response in the present study, it is speculated that alternative modes of action are recruited for TET and TMT. During mitoenergetic dysfunction, the balance between glycolytic and mitochondrial ATP generation is crucial for cell survival. A loss in mitochondrial ATP production is compensated for by pyruvate metabolism into lactate (Bonora et al. 2012; Lieburg-Apers et al. 2015). However, the lower levels observed for TETBr in ATP-linked respiration was accompanied by a lower, rather than higher, glycolytic rate. The recent work by Tannahill et al. (2013) showing an altered LPS-induced IL-1 response with pharmacological inhibition of glycolysis might provide a basis for this difference. Given that alterations in mitochondria can modify a cell's ability to respond to inflammatory signals, we shifted the exposure paradigm to examine alterations in the response to LPS or to LPS+ATP in exposed cells. Under this paradigm, we observed no effect on *Tnfα* but did observe a significant inhibition of *Il1a* and *Il1b* induction, demonstrating a low-level effect on proper macrophage response to a pro-inflammatory stimulus and suggestive of immunodeficiency.

NLRP3 inflammasome activation has been linked to the recognition of mitochondrial danger signals and the generation of mtROS (Cruz et al. 2007; Nanayakkara et al. 2019) with many identified NLRP3 inflammasome activators shown to also trigger mtROS production (Tschopp and Schroder 2010). We now report that neither tri-organotin elevated cellular nor mtROS, which would exclude mtROS elevation as a critical factor in inflammasome activation. This would be within the support for both mtROS-dependent and ROS-independent activation mechanisms (Jabaut et al. 2013; Muñoz-Planillo et al. 2013; Sanman et al. 2016). In addition to mtROS activation, mitochondrial function as well as nitric oxide have been shown as being important for regulating NLRP3 inflammasome activation and IL-1β release (Hernandez-Cuellar et al. 2012; Mao et al. 2013; Tran and Kitami 2019). However, in the present study, a prominent role for ROS or nitric oxide was not identified. One possible alternative mechanism for the NLRP3 inflammasome aggregate formation may be related to alterations in ion channels or elevated ion permeability due to membrane damage (Di Virgilio et al. 2018; Hafner-Bratkovič and Pelegrín 2018). Particulate activators can induce NLRP3 inflammasome through a sequence of events involving extracellular release of ATP through hemichannel opening and signaling through P2XRs. Membrane pore formation can trigger K^+ efflux and extracellular ATP to engage P2RX7 (Franceschini et al. 2015; Kahlenberg and Dubyak 2004; Mariathasan et al. 2006). When released into the extracellular space, ATP functions as a ubiquitous DAMP, acting at the metabotropic G-protein-coupled P2Y-receptors and the ionotropic P2RX7 for NLRP3 inflammasome activation and ATP-dependent K^+ efflux activation (Di Virgilio et al. 2018; Franceschini et al. 2015; Gombault et al. 2013; Hafner-Bratkovič and Pelegrín 2018). P2X7 receptors are frequently expressed with another P2X receptor subtype, P2X4, with which they can form heteromeric receptors (Guo et al. 2007). Decreasing levels of P2X4 have been linked as a mechanism to minimize P2X7 receptor-mediated cell death by lowering intracellular Ca^{2+} (Kawano et al. 2012) and may account for the differences observed with TETBr. TET and TMT are effective inhibitors of ATP activated by Na^+ and K^+ (Na^+-K^+-ATPase) (Aschner and Aschner 1992). Alterations in K^+ may contribute to the subtle NLRP3 inflammasome assembly observed with TETBr in non-primed cells and the elevation in *P2rx7* seen with priming. In addition, the diminished but not eliminated response with apyrase further suggests a role for K^+ efflux. Although this data would imply higher levels of extracellular ATP, this interpretation requires caution given that commercially available apyrase preparations reportedly contain K^+ levels that are sufficient to inhibit NLRP3 activation (Muñoz-Planillo et al. 2013; Madry et al. 2018). In comparison, TMT inhibits K^+ influx (Aschner et al. 1992), which may account for the difference in direct induction of ASC speck formation as compared with TETBr. These findings suggest that tri-organotins can serve as effective inflammasome triggering agents in LPS-primed cells. Although the levels are low, the relative levels observed were within ranges previously reported for NLRP3 inflammasome activation in macrophages following oxidized low-density lipoprotein (Sheedy et al. 2013) or silica (Dostert et al. 2008).

miRNAs serve as major players in the regulation of NLRP3 inflammasome activation at both the priming and secondary trigger steps (O'Neill et al. 2011; Rebane and Akdis 2013; Zamani et al. 2020). This tight regulation is dependent upon the inhibitory effects of miRNAs on inflammatory processes (Coll and O'Neill 2010) as a negative feedback mechanism to down-modulate inflammatory cytokine production (Ceppi et al. 2009). Several miRNAs have been demonstrated to target mRNA transcripts of genes coding for components of the NLRP3 inflammasome complex (Bauernfeind et al. 2012; Boxberger et al. 2019; Tezcan et al. 2019; Zamani et al. 2020). Although a priming stimulus triggers NLRP3 transcription, protein translation can be interrupted by binding of miRNAs (*miR-223*, *miR-22*, *miR-30e*, and *miR-7*) to the untranslated region. In contrast, lower expression of miRNAs, such as *miR-7* and *miR-30e*, may lead to a loss of regulatory control of NLRP3 activation (Li et al. 2018). Given that both TETBr and TMTOH were able to serve as secondary triggers for ASC complex assembly and IL-1β release, it was of interest that differences in only four miRNAs were common to both, with one, *miR-151-3p*, lower and three (*miR-6909-5p*, *miR-7044-5p*, and *miR-7686-5p*) higher. Little is known regarding these specific miRNA species, with the exception of *miR-7686-5p* and *miR-151-3p. miR-7686-5p* has been reported to be up-regulated in the testes of mice exposed to a mixture of environmental endocrine disruptors (Buñay et al. 2017). *miR-151-3p* has recently been shown to contribute to LPS-stimulated up-regulation of STAT3 and IL-6 production (Liu et al. 2018a). Differences observed in LPS-primed cells were supported by the gene expression array identifying the STAT3 signaling pathway. Functional analysis of the targets for shared miRNAs also included signaling pathways for apoptosis, Wnt beta-catenin, the pro-inflammatory cytokine IL-12 and the IL-10 family of anti-inflammatory cytokines (IL-10, IL-22). IL-12 can signal for the activation of STATs (Trinchieri 2003); however, IL-10 serves as a negative regulator of IL-12 (Aste-Amezaga et al. 1998) and can inhibit NLRP3 inflammasome activation by reducing mtROS production (Ip et al. 2017). Thus, the overall profiles suggested an active cellular process to regulate the overall inflammatory response and to facilitate cell survival. This would be consistent with the growing body of evidence suggesting a threshold of NLRP3 activity acting as a safeguard mechanism to prevent inflammasome overactivation (Bortolotti et al. 2018). Additional experiments based upon the differential profiles generated by the tri-organotin compounds and the level of inflammasome activation may help to identify pivot points of this threshold and provide a framework for examining associations between various mitochondrial toxicants and immune dysfunction. One pivotal point may be

at the (de)ubiquitinating enzyme A20 or TNFα-induced protein 3 (*Tnfaip3, A20/tnfaip3*), a target gene of let-7, *miR-125a*, *miR-125b*, which regulates crucial stages in immune cell homeostasis, such as NF-κB activation and apoptosis, and directly influences NLRP3 inflammasome in macrophages (Duong et al. 2015; Vande Walle et al. 2014).

Overall, the data suggests that these specific tri-organotins, TMTOH and TETBr, which are known as mitochondrial toxicants, can serve as secondary triggers for NLRP3 inflammasome activation; however, the driving underlying mechanism remains in question. Differences between tri-organotins were demonstrated in mitochondrial bioenergetics, inflammasome activation, molecular profiles, and LPS response. The excess stimulation with TETBr suggested that aspects of this response reflected cell survival mechanisms involving an integrated stress response (Pakos-Zebrucka et al. 2016). Thus, the outcome likely depends on severity, number of cells recruited, secondary stimulatory factors such as ion-channel function, and recruitment of cell survival pathways. With NLRP3 inflammasome activation, inflammatory contribution of IL-1β and IL-18 is clear; however, with pyroptosis, the excretion of exosomes (Zhang et al. 2017; Cypryk et al. 2018) and oligomeric NLRP3 inflammasome particles (Baroja-Mazo et al. 2014; Franklin et al. 2014) are factors that act upon adjacent cells to activate the NF-κB signal pathway, alter lysosome integrity, and enhance or prolong the immune response (Venegas et al. 2017). Each of these factors may represent a biological process of concern for downstream adverse effects.

Using a relatively high-throughput live-cell imaging approach adapted from pharmaceutical inflammasome-activation screening approaches (Redondo-Castro et al. 2018), we provide data suggesting that environmental factors with mitotoxic properties may serve as secondary triggers for inflammasome activation at levels that fail to induce a pro-inflammatory response. It is likely that, although a mitochondrial component may be associated with this immune cell response, it is not a defining characteristic. Thus, examination of NLRP3 inflammasome activation may offer an approach for examining downstream events distinguishing between mitotoxicants, or other classes of compounds, suspected of producing immune cell dysfunction. Further examination of chemical classes with mitochondrial activity is required to determine whether this approach can be used to develop a causal link and biological hierarchy leading to adverse health effects given the critical need for appropriate immune cell functioning.

Acknowledgments

The authors acknowledge the expert assistance of the Viral Vector Core and K. Gerrish of the Molecular Genomics Core Laboratories of the National Institute of Environmental Health Sciences/National Institutes of Health (NIEHS/NIH); L. Wyrick and A. Krause for graphics; and D. R. Germolec, S. Garantziotis, and C.A. McPherson for their review of the manuscript. This research was supported by the Division National Toxicology Program and Division of Intramural Research, NIEHS/NIH, intramural research funding Z01 ES021164 and Z01 ES102005.

References

Abais JM, Xia M, Zhang Y, Boini KM, Li PL. 2015. Redox regulation of NLRP3 inflammasomes: ROS as trigger or effector? Antioxid Redox Signal 22(13):1111–1129, PMID: 25330206, https://doi.org/10.1089/ars.2014.5994.

Aldridge WN, Street BW, Noltes JG. 1981. The action of 5-coordinate triorganotin compounds on rat liver mitochondria. Chem Biol Interact 34(2):223–232, PMID: 7460084, https://doi.org/10.1016/0009-2797(81)90133-2.

Aldridge WN, Street BW, Skilleter DN. 1977. Oxidative phosphorylation. Halide-dependent and halide-independent effects of triorganotin and trioganolead compounds on mitochondrial functions. Biochem J 168(3):353–364, PMID: 24436, https://doi.org/10.1042/bj1680353.

Aschner M, Aschner JL. 1992. Cellular and molecular effects of trimethyltin and triethyltin: relevance to organotin neurotoxicity. Neurosci Biobehav Rev 16(4):427–435, PMID: 1480339, https://doi.org/10.1016/s0149-7634(05)80184-8.

Aschner M, Gannon M, Kimelberg HK. 1992. Interactions of trimethyl tin (TMT) with rat primary astrocyte cultures: altered uptake and efflux of rubidium, L-glutamate and D-aspartate. Brain Res 582(2):181–185, PMID: 1356582, https://doi.org/10.1016/0006-8993(92)90131-r.

Aste-Amezaga M, Ma X, Sartori A, Trinchieri G. 1998. Molecular mechanisms of the induction of IL-12 and its inhibition by IL-10. J Immunol 160(12):5936–5944, PMID: 9637507.

Attahiru US, Iyaniwura TT, Adaudi AO, Bonire JJ. 1991. Subchronic toxicity studies of tri-n-butyltin and triphenyltin acetates in rats. Vet Hum Toxicol 33(5):499–502, PMID: 1746148.

Attene-Ramos MS, Huang R, Michael S, Witt KL, Richard A, Tice RR, et al. 2015. Profiling of the Tox21 chemical collection for mitochondrial function to identify compounds that acutely decrease mitochondrial membrane potential. Environ Health Perspect 123(1):49–56, PMID: 25302578, https://doi.org/10.1289/ehp.1408642.

Barde I, Salmon P, Trono D. 2010. Production and titration of lentiviral vectors. Curr Protoc Neurosci 53(1):4.21.1–4.21.23, PMID: 20938923, https://doi.org/10.1002/0471142301.ns0421s53.

Barnes JM, Stoner HB. 1959. The toxicity of tin compounds. Pharmacol Rev 11:211, PMID: 13667399.

Baroja-Mazo A, Martín-Sánchez F, Gomez AI, Martínez CM, Amores-Iniesta J, Compan V, et al. 2014. The NLRP3 inflammasome is released as a particulate danger signal that amplifies the inflammatory response. Nat Immunol 15(8):738–748, PMID: 24952504, https://doi.org/10.1038/ni.2919.

Barrey E, Saint-Auret G, Bonnamy B, Damas D, Boyer O, Gidrol X, et al. 2011. Pre-microRNA and mature microRNA in human mitochondria. PLoS One 6(5):e20220, PMID: 21637849, https://doi.org/10.1371/journal.pone.0020220.

Bauernfeind FG, Horvath G, Stutz A, Alnemri ES, MacDonald K, Speert D, et al. 2009. Cutting edge: NF-κB activating pattern recognition and cytokine receptors license NLRP3 inflammasome activation by regulating NLRP3 expression. J Immunol 183(2):787–791, PMID: 19570822, https://doi.org/10.4049/jimmunol.0901363.

Bauernfeind F, Rieger A, Schildberg FA, Knolle PA, Schmid-Burgk JL, Hornung V, et al. 2012. NLRP3 inflammasome activity is negatively controlled by miR-223. J Immunol 189(8):4175–4181, PMID: 22984082, https://doi.org/10.4049/jimmunol.1201516.

Benjamini Y, Hochberg Y. 1995. Controlling the false discovery rate: a practical and powerful approach to multiple testing. J R Stat Soc Ser B: Methodological 57(1):289–300, https://doi.org/10.1111/j.2517-6161.1995.tb02031.x.

Benya TJ. 1997. Bis(tributyltin) oxide toxicology. Drug Metab Rev 29(4):1189–1280, PMID: 9421689, https://doi.org/10.3109/03602539709002247.

Bhatt K, Lanting LL, Jia Y, Yadav S, Reddy MA, Magilnick N, et al. 2016. Anti-inflammatory role of microRNA-146a in the pathogenesis of diabetic nephropathy. J Am Soc Nephrol 27(8):2277–2288, PMID: 26647423, https://doi.org/10.1681/ASN.2015010111.

Bian Z, Li LM, Tang R, Hou DX, Chen X, Zhang CY, et al. 2010. Identification of mouse liver mitochondria-associated miRNAs and their potential biological functions. Cell Res 20(9):1076–1078, PMID: 20733615, https://doi.org/10.1038/cr.2010.119.

Bonora M, Patergnani S, Rimessi A, De Marchi E, Suski JM, Bononi A, et al. 2012. ATP synthesis and storage. Purinergic Signal 8(3):343–357, PMID: 22528680, https://doi.org/10.1007/s11302-012-9305-8.

Bortolotti P, Faure E, Kipnis E. 2018. Inflammasomes in tissue damages and immune disorders after trauma. Front Immunol 9:1900, PMID: 30166988, https://doi.org/10.3389/fimmu.2018.01900.

Boursereau R, Abou-Samra M, Lecompte S, Noel L, Brichard SM. 2018. Downregulation of the NLRP3 inflammasome by adiponectin rescues Duchenne muscular dystrophy. BMC Biol 16(1):33, PMID: 29558930, https://doi.org/10.1186/s12915-018-0501-z.

Bowen C, Childers G, Perry C, Martin N, McPherson CA, Lauten T, et al. 2020. Mitochondrial-related effects of pentabromophenol, tetrabromobisphenol A, and triphenyl phosphate on murine BV-2 microglia cells. Chemosphere 255:126919, PMID: 32402876, https://doi.org/10.1016/j.chemosphere.2020.126919.

Boxberger N, Hecker M, Zettl UK. 2019. Dysregulation of inflammasome priming and activation by microRNAs in human immune-mediated diseases. J Immunol 202(8):2177–2187, PMID: 30962309, https://doi.org/10.4049/jimmunol.1801416.

Brown S, Wilburn W, Martin T, Whalen M. 2018. Butyltin compounds alter secretion of interleukin 6 from human immune cells. J Appl Toxicol 38(2):201–218, PMID: 28840599, https://doi.org/10.1002/jat.3514.

Broz P, Dixit VM. 2016. Inflammasomes: mechanism of assembly, regulation and signalling. Nat Rev Immunol 16(7):407–420, PMID: 27291964, https://doi.org/10.1038/nri.2016.58.

Buñay J, Larriba E, Moreno RD, Del Mazo J. 2017. Chronic low-dose exposure to a mixture of environmental endocrine disruptors induces microRNAs/isomiRs deregulation in mouse concomitant with intratesticular estradiol reduction. Sci Rep 7(1):3373, PMID: 28611354, https://doi.org/10.1038/s41598-017-02752-7.

Caito SW, Aschner M. 2015. Mitochondrial redox dysfunction and environmental exposures. Antioxid Redox Signal 23(6):578–595, PMID: 25826672, https://doi.org/10.1089/ars.2015.6289.

Cassel SL, Joly S, Sutterwala FS. 2009. The NLRP3 inflammasome: a sensor of immune danger signals. Semin Immunol 21(4):194–198, PMID: 19501527, https://doi.org/10.1016/j.smim.2009.05.002.

Ceppi M, Pereira PM, Dunand-Sauthier I, Barras E, Reith W, Santos MA, et al. 2009. MicroRNA-155 modulates the interleukin-1 signaling pathway in activated human monocyte-derived dendritic cells. Proc Natl Acad Sci U S A 106(8):2735–2740, PMID: 19193853, https://doi.org/10.1073/pnas.0811073106.

Chen D, Dixon BJ, Doycheva DM, Li B, Zhang Y, Hu Q, et al. 2018. IRE1α inhibition decreased TXNIP/NLRP3 inflammasome activation through miR-17-5p after neonatal hypoxic-ischemic brain injury in rats. J Neuroinflammation 15(1):32, PMID: 29394934, https://doi.org/10.1186/s12974-018-1077-9.

Chen H, Lu Q, Fei X, Shen L, Jiang D, Dai D, et al. 2016. miR-22 inhibits the proliferation, motility, and invasion of human glioblastoma cells by directly targeting SIRT1. Tumor Biol 37(5):6761–6768, PMID: 26662303, https://doi.org/10.1007/s13277-015-4575-8.

Coll RC, O'Neill LA. 2010. New insights into the regulation of signalling by Toll-like receptors and Nod-like receptors. J Innate Immun 2(5):406–421, PMID: 20505309, https://doi.org/10.1159/000315469.

Cristòfol RM, Gassó S, Vílchez D, Pertusa M, Rodríguez-Farré E, Sanfeliu C, et al. 2004. Neurotoxic effects of trimethyltin and triethyltin on human fetal neuron and astrocyte cultures: a comparative study with rat neuronal cultures and human cell lines. Toxicol Lett 152(1):35–46, PMID: 15294345, https://doi.org/10.1016/j.toxlet.2004.03.023.

Cruz CM, Rinna A, Forman HJ, Ventura ALM, Persechini PM, Ojcius DM, et al. 2007. ATP activates a reactive oxygen species-dependent oxidative stress response and secretion of proinflammatory cytokines in macrophages. J Biol Chem 282(5):2871–2879, PMID: 17132626, https://doi.org/10.1074/jbc.M608083200.

Cypryk W, Nyman TA, Matikainen S. 2018. From inflammasome to exosome—does extracellular vesicle secretion constitute an inflammasome-dependent immune response? Front Immunol 9:2188, PMID: 30319640, https://doi.org/10.3389/fimmu.2018.02188.

Darley-Usmar VM, Rickwood D, Wilson MT. 1987. *Mitochondria: a Practical Approach*. Oxford; Washington, DC: IRL Press.

Davidson CE, Reese BE, Billingsley ML, Yun JK. 2004. Stannin, a protein that localizes to the mitochondria and sensitizes NIH-3T3 cells to trimethyltin and dimethyltin in toxicity. Mol Pharmacol 66(4):855–863, PMID: 15269288, https://doi.org/10.1124/mol.104.001719.

Deets KA, Vance RE. 2021. Inflammasomes and adaptive immune responses. Nat Immunol 22(4):412–422, PMID: 33603227, https://doi.org/10.1038/s41590-021-00869-6.

Dela Cruz CS, Kang MJ. 2018. Mitochondrial dysfunction and damage associated molecular patterns (DAMPs) in chronic inflammatory diseases. Mitochondrion 41:37–44, PMID: 29221810, https://doi.org/10.1016/j.mito.2017.12.001.

Delp J, Funke M, Rudolf F, Cediel A, Bennekou SH, van der Stel W, et al. 2019. Development of a neurotoxicity assay that is tuned to detect mitochondrial toxicants. Arch Toxicol 93(6):1585–1608, PMID: 31190196, https://doi.org/10.1007/s00204-019-02473-y.

Di Virgilio F, Schmalzing G, Markwardt F. 2018. The elusive P2X7 macropore. Trends Cell Biol 28(5):392–404, PMID: 29439897, https://doi.org/10.1016/j.tcb.2018.01.005.

Dinarello CA. 2009. Immunological and inflammatory functions of the interleukin-1 family. Annu Rev Immunol 27:519–550, PMID: 19302047, https://doi.org/10.1146/annurev.immunol.021908.132612.

Dinarello CA. 2011. A clinical perspective of IL-1β as the gatekeeper of inflammation. Eur J Immunol 41(5):1203–1217, PMID: 21523780, https://doi.org/10.1002/eji.201141550.

Dostert C, Pétrilli V, Van Bruggen R, Steele C, Mossman BT, Tschopp J, et al. 2008. Innate immune activation through Nalp3 inflammasome sensing of asbestos and silica. Science 320(5876):674–677, PMID: 18403674, https://doi.org/10.1126/science.1156995.

Dreier DA, Mello DF, Meyer JN, Martyniuk CJ. 2019. Linking mitochondrial dysfunction to organismal and population health in the context of environmental pollutants: progress and considerations for mitochondrial adverse outcome pathways. Environ Toxicol Chem 38(8):1625–1634, PMID: 31034624, https://doi.org/10.1002/etc.4453.

Duewell P, Kono H, Rayner KJ, Sirois CM, Vladimer G, Bauernfeind FG, et al. 2010. NLRP3 inflammasomes are required for atherogenesis and activated by cholesterol crystals. Nature 464(7293):1357–1361, PMID: 20428172, https://doi.org/10.1038/nature08938.

Duong BH, Onizawa M, Oses-Prieto JA, Advincula R, Burlingame A, Malynn BA, et al. 2015. A20 restricts ubiquitination of pro-interleukin-1β protein complexes and suppresses NLRP3 inflammasome activity. Immunity 42(1):55–67, PMID: 25607459, https://doi.org/10.1016/j.immuni.2014.12.031.

EFSA (European Food Safety Authority). 2004. Opinion of the Scientific Panel on contaminants in the food chain [CONTAM] on a request from the commission to assess the health risks to consumers associated with exposure to organotins in foodstuffs. EFSA J 102:1–119, https://doi.org/10.2903/j.efsa.2004.102.

Eisenbarth SC, Colegio OR, O'Connor W, Sutterwala FS, Flavell RA. 2008. Crucial role for the Nalp3 inflammasome in the immunostimulatory properties of aluminum adjuvants. Nature 453(7198):1122–1126, PMID: 18496530, https://doi.org/10.1038/nature06939.

Ferraz da Silva I, Freitas-Lima LC, Graceli JB, Rodrigues LCM. 2018. Organotins in neuronal damage, brain function, and behavior: a short review. Front Endocrinol (Lausanne) 8:366, PMID: 29358929, https://doi.org/10.3389/fendo.2017.00366.

Fontan MM, Verger, Pery, Loiseau, Mulon. 1955. Quatre cas dont deux mortels d'intoxication par le "Stalinon" chez l'enfant. J Med Bord 132:399–405, PMID: 14381804.

Franceschini A, Capece M, Chiozzi P, Falzoni S, Sanz JM, Sarti AC, et al. 2015. The P2X7 receptor directly interacts with the NLRP3 inflammasome scaffold protein. FASEB J 29(6):2450–2461, PMID: 25690658, https://doi.org/10.1096/fj.14-268714.

Franchi L, Eigenbrod T, Muñoz-Planillo R, Nuñez G. 2009. The inflammasome: a caspase-1-activation platform that regulates immune responses and disease pathogenesis. Nat Immunol 10(3):241–247, PMID: 19221555, https://doi.org/10.1038/ni.1703.

Franklin BS, Bossaller L, De Nardo D, Ratter JM, Stutz A, Engels G, et al. 2014. The adaptor ASC has extracellular and 'prionoid' activities that propagate inflammation. Nat Immunol 15(8):727–737, PMID: 24952505, https://doi.org/10.1038/ni.2913.

Ganeshan K, Chawla A. 2014. Metabolic regulation of immune responses. Annu Rev Immunol 32:609–634, PMID: 24655299, https://doi.org/10.1146/annurev-immunol-032713-120236.

Gennari A, Viviani B, Galli CL, Marinovich M, Pieters R, Corsini E, et al. 2000. Organotins induce apoptosis by disturbance of $[Ca^{2+}]_i$ and mitochondrial activity, causing oxidative stress and activation of caspases in rat thymocytes. Toxicol Appl Pharmacol 169(2):185–190, PMID: 11097871, https://doi.org/10.1006/taap.2000.9076.

Ghiringhelli F, Apetoh L, Tesniere A, Aymeric L, Ma Y, Ortiz C, et al. 2009. Activation of the NLRP3 inflammasome in dendritic cells induces IL-1β-dependent adaptive immunity against tumors. Nat Med 15(10):1170–1178, PMID: 19767732, https://doi.org/10.1038/nm.2028.

Gombault A, Baron L, Couillin I. 2013. ATP release and purinergic signaling in NLRP3 inflammasome activation. Front Immunol 3:414, PMID: 23316199, https://doi.org/10.3389/fimmu.2012.00414.

Gomez FD, Apodaca P, Holloway LN, Pannell KH, Whalen MM. 2007. Effect of a series of triorganotins on the immune function of human natural killer cells. Environ Toxicol Pharmacol 23(1):18–24, PMID: 21783732, https://doi.org/10.1016/j.etap.2006.06.001.

Goodchild CG, Simpson AM, Minghetti M, DuRant SE. 2019. Bioenergetics-adverse outcome pathway: linking organismal and suborganismal energetic endpoints to adverse outcomes. Environ Toxicol Chem 38(1):27–45, PMID: 30259559, https://doi.org/10.1002/etc.4280.

Gross O, Thomas CJ, Guarda G, Tschopp J. 2011. The inflammasome: an integrated view. Immunol Rev 243(1):136–151, PMID: 21884173, https://doi.org/10.1111/j.1600-065X.2011.01046.x.

Guo C, Masin M, Qureshi OS, Murrell-Lagnado RD. 2007. Evidence for functional $P2X_4/P2X_7$ heteromeric receptors. Mol Pharmacol 72(6):1447–1456, PMID: 17785580, https://doi.org/10.1124/mol.107.035980.

Guo H, Callaway JB, Ting JPY. 2015. Inflammasomes: mechanism of action, role in disease, and therapeutics. Nat Med 21(7):677–687, PMID: 26121197, https://doi.org/10.1038/nm.3893.

Hafner-Bratkovič I, Pelegrín P. 2018. Ion homeostasis and ion channels in NLRP3 inflammasome activation and regulation. Curr Opin Immunol 52:8–17, PMID: 29555598, https://doi.org/10.1016/j.coi.2018.03.010.

Harford AJ, O'Halloran K, Wright PEA. 2007. Effect of in vitro and in vivo organotin exposures on the immune functions of Murray cod (*maccullochella peelii peelii*). Environ Toxicol Chem 26(8):1649–1656, PMID: 17702338, https://doi.org/10.1897/06-449r.1.

Harry GJ, Bruccoleri A, Lefebvre d'Hellencourt C. 2003. Differential modulation of hippocampal chemical-induced injury response by ebselen, pentoxifylline, and TNFα-, IL-1α-, IL-6-neutralizing antibodies. J Neurosci Res 73(4):526–536, PMID: 12898537, https://doi.org/10.1002/jnr.10653.

Hernandez-Cuellar E, Tsuchiya K, Hara H, Fang R, Sakai S, Kawamura I, et al. 2012. Cutting edge: nitric oxide inhibits the NLRP3 inflammasome. J Immunol 189(11):5113–5117, PMID: 23100513, https://doi.org/10.4049/jimmunol.1202479.

Holloway LN, Pannell KH, Whalen MM. 2008. Effects of a series of triorganotins on ATP levels in human natural killer cells. Environ Toxicol Pharmacol 25(1):43–50, PMID: 19122738, https://doi.org/10.1016/j.etap.2007.08.008.

Hou J, Xue J, Lee M, Sung C. 2017. Ginsenoside Rd as a potential neuroprotective agent prevents trimethyltin injury. Biomed Rep 6(4):435–440, PMID: 28413642, https://doi.org/10.3892/br.2017.864.

Huang WQ, Wei P, Lin RQ, Huang F. 2017. Protective effects of microrna-22 against endothelial cell injury by targeting NLRP3 through suppression of the inflammasome signaling pathway in a rat model of coronary heart disease. Cell Physiol Biochem 43(4):1346–1358, PMID: 28992621, https://doi.org/10.1159/000481846.

Hughes MM, O'Neill LAJ. 2018. Metabolic regulation of NLRP3. Immunol Rev 281(1):88–98, PMID: 29247992, https://doi.org/10.1111/imr.12608.

Im E, Kim H, Kim J, Lee H, Yang H. 2015. Tributyltin acetate-induced immunotoxicity is related to inhibition of T cell development in the mouse thymus. Mol Cell Toxicol 11(2):231–239, https://doi.org/10.1007/s13273-015-0022-6.

Ip WKE, Hoshi N, Shouval DS, Snapper S, Medzhitov R. 2017. Anti-inflammatory effect of IL-10 mediated by metabolic reprogramming of macrophages. Science 356(6337):513–519, PMID: 28473584, https://doi.org/10.1126/science.aal3535.

Jabaut J, Ather JL, Taracanova A, Poynter ME, Ckless K. 2013. Mitochondria-targeted drugs enhance Nlrp3 inflammasome-dependent IL-1β secretion in association with alterations in cellular redox and energy status. Free Radic Biol Med 60:233–245, PMID: 23376234, https://doi.org/10.1016/j.freeradbiomed.2013.01.025.

Javadov S, Kozlov AV, Camara AKS. 2020. Mitochondria in health and diseases. Cells 9(5):1177, PMID: 32397376, https://doi.org/10.3390/cells9051177.

Johansson AC, Appelqvist H, Nilsson C, Kågedal K, Roberg K, Ollinger K. 2010. Regulation of apoptosis-associated lysosomal membrane permeabilization. Apoptosis 15(5):527–540, PMID: 20077016, https://doi.org/10.1007/s10495-009-0452-5.

Kahlenberg JM, Dubyak GR. 2004. Mechanisms of caspase-1 activation by P2X7 receptor-mediated K^+ release. Am J Physiol Cell Physiol 286(5):C1100–C1108, PMID: 15075209, https://doi.org/10.1152/ajpcell.00494.2003.

Kaneko N, Kurata M, Yamamoto T, Morikawa S, Masumoto J. 2019. The role of interleukin-1 in general pathology. Inflamm Regen 39:12, PMID: 31182982, https://doi.org/10.1186/s41232-019-0101-5.

Kawano A, Tsukimoto M, Noguchi T, Hotta N, Harada H, Takenouchi T, et al. 2012. Involvement of P2X4 receptor in P2X7 receptor-dependent cell death of mouse macrophages. Biochem Biophys Res Commun 419(2):374–380, PMID: 22349510, https://doi.org/10.1016/j.bbrc.2012.01.156.

Kelley N, Jeltema D, Duan Y, He Y. 2019. The NLRP3 inflammasome: an overview of mechanisms of activation and regulation. Int J Mol Sci 20(13):3328, PMID: 31284572, https://doi.org/10.3390/ijms20133328.

Khan NA, Govindaraj P, Meena AK, Thangaraj K. 2015. Mitochondrial disorders: challenges in diagnosis & treatment. Indian J Med Res 141(1):13–26, PMID: 25857492, https://doi.org/10.4103/0971-5916.154489.

Kraft AD, McPherson CA, Harry GJ. 2016. Association between microglia, inflammatory factors, and complement with loss of hippocampal mossy fiber synapses induced by trimethyltin. Neurotox Res 30(1):53–66, PMID: 26892644, https://doi.org/10.1007/s12640-016-9606-8.

Kren BT, Wong PYP, Sarver A, Zhang X, Zeng Y, Steer CJ. 2009. MicroRNAs identified in highly purified liver-derived mitochondria may play a role in apoptosis. RNA Biol 6(1):65–72, PMID: 19106625, https://doi.org/10.4161/rna.6.1.7534.

Lawrence S, Pellom ST Jr, Shanker A, Whalen MM. 2016. Tributyltin exposure alters cytokine levels in mouse serum. J Immunotoxicol 13(6):870–878, PMID: 27602597, https://doi.org/10.1080/1547691X.2016.1221867.

Li D, Yang H, Ma J, Luo S, Chen S, Gu Q. 2018. MicroRNA-30e regulates neuroinflammation in MPTP model of Parkinson's disease by targeting Nlrp3. Hum Cell 31(2):106–115, PMID: 29274035, https://doi.org/10.1007/s13577-017-0187-5.

Liemburg-Apers DC, Schirris TJJ, Russel FGM, Willems PHGM, Koopman WJH. 2015. Mitoenergetic dysfunction triggers a rapid compensatory increase in steady-state glucose flux. Biophys J 109(7):1372–1386, PMID: 26445438, https://doi.org/10.1016/j.bpj.2015.08.002.

Liu Q, Zhang D, Hu D, Zhou X, Zhou Y. 2018a. The role of mitochondria in NLRP3 inflammasome activation. Mol Immunol 103:115–124, PMID: 30248487, https://doi.org/10.1016/j.molimm.2018.09.010.

Liu X, Su X, Xu S, Wang H, Han D, Li J, et al. 2018b. MicroRNA *in vivo* precipitation identifies miR-151-3p as a computational unpredictable miRNA to target *Stat3* and inhibits innate IL-6 production. Cell Mol Immunol 15(2):99–110, PMID: 28890541, https://doi.org/10.1038/cmi.2017.82.

Liu W, Yin Y, Zhou Z, He M, Dai Y. 2014. OxLDL-induced IL-1beta secretion promoting foam cells formation was mainly via CD36 mediated ROS production leading to NLRP3 inflammasome activation. Inflamm Res 63(1):33–43, PMID: 24121974, https://doi.org/10.1007/s00011-013-0667-3.

Long J, Wang Q, He H, Sui X, Lin G, Wang S, et al. 2019. NLRP3 inflammasome activation is involved in trimethyltin-induced neuroinflammation. Brain Res 1718:186–193, PMID: 31059678, https://doi.org/10.1016/j.brainres.2019.05.003.

Lunov O, Syrovets T, Loos C, Nienhaus GU, Mailänder V, Landfester K, et al. 2011. Amino-functionalized polystyrene nanoparticles activate the NLRP3 inflammasome in human macrophages. ACS Nano 5(12):9648–9657, PMID: 22111911, https://doi.org/10.1021/nn203596e.

Lynch MA. 2020. Can the emerging field of immunometabolism provide insights into neuroinflammation? Prog Neurobiol 184:101719, PMID: 31704314, https://doi.org/10.1016/j.pneurobio.2019.101719.

Madry C, Arancibia-Cárcamo IL, Kyrargyri V, Chan VTT, Hamilton NB, Attwell D, et al. 2018. Effects of the ecto-ATPase apyrase on microglial ramification and surveillance reflect cell depolarization, not ATP depletion. Proc Natl Acad Sci U S A 115(7):E1608–E1617, PMID: 29382767, https://doi.org/10.1073/pnas.1715354115.

Mao K, Chen S, Chen M, Ma Y, Wang Y, Huang B, et al. 2013. Nitric oxide suppresses NLRP3 inflammasome activation and protects against LPS-induced septic shock. Cell Res 23(2):201–212, PMID: 23318584, https://doi.org/10.1038/cr.2013.6.

Mariathasan S, Weiss DS, Newton K, McBride J, O'Rourke K, Roose-Girma M, et al. 2006. Cryopyrin activates the inflammasome in response to toxins and ATP. Nature 440(7081):228–232, PMID: 16407890, https://doi.org/10.1038/nature04515.

Martinon F, Burns K, Tschopp J. 2002. The inflammasome: a molecular platform triggering activation of inflammatory caspases and processing of proIL-β. Mol Cell 10(2):417–426, PMID: 12191486, https://doi.org/10.1016/S1097-2765(02)00599-3.

Martinon F, Pétrilli V, Mayor A, Tardivel A, Tschopp J. 2006. Gout-associated uric acid crystals activate the NALP3 inflammasome. Nature 440(7081):237–241, PMID: 16407889, https://doi.org/10.1038/nature04516.

Mathur A, Hayward JA, Man SM. 2018. Molecular mechanisms of inflammasome signaling. J Leukoc Biol 103(2):233–257, PMID: 28855232, https://doi.org/10.1189/jlb.3MR0617-250R.

Meyer JN, Leung MCK, Rooney JP, Sendoel A, Hengartner MO, Kisby GE, et al. 2013. Mitochondria as a target of environmental toxicants. Toxicol Sci 134(1):1–17, PMID: 23629515, https://doi.org/10.1093/toxsci/kft102.

Muñoz-Planillo R, Kuffa P, Martínez-Colón G, Smith BL, Rajendiran TM, Núñez G. 2013. K^+ efflux is the common trigger of NLRP3 inflammasome activation by bacterial toxins and particulate matter. Immunity 38(6):1142–1153, PMID: 23809161, https://doi.org/10.1016/j.immuni.2013.05.016.

Mushak P, Krigman MR, Mailman RB. 1982. Comparative organotin toxicity in the developing rat: somatic and morphological changes and relationship to accumulation of total tin. Neurobehav Tox Teratol 4(2):209–215, PMID: 7088250.

Nakahira K, Haspel JA, Rathinam VAK, Lee SJ, Dolinay T, Lam HC, et al. 2011. Autophagy proteins regulate innate immune responses by inhibiting the release of mitochondrial DNA mediated by the NALP3 inflammasome. Nat Immunol 12(3):222–230, PMID: 21151103, https://doi.org/10.1038/ni.1980.

Nanayakkara GK, Wang H, Yang X. 2019. Proton leak regulates mitochondrial reactive oxygen species generation in endothelial cell activation and inflammation—a novel concept. Arch Biochem Biophys 662:68–74, PMID: 30521782, https://doi.org/10.1016/j.abb.2018.12.002.

Nesci S, Ventrella V, Trombetti F, Pirini M, Borgatti AR, Pagliarani A, et al. 2011. Tributyltin (TBT) and dibutyltin (DBT) differently inhibit the mitochondrial Mg-ATPase activity in mussel digestive gland. Toxicol In Vitro 25(1):117–124, PMID: 20950683, https://doi.org/10.1016/j.tiv.2010.10.001.

Nunes-Silva A, Dittz D, Santana HS, Faria RA, Freitas KM, Coutinho CR, et al. 2018. The pollutant organotins leads to respiratory disease by inflammation: a mini-review. Front Endocrinol (Lausanne) 8:369, PMID: 29403432, https://doi.org/10.3389/fendo.2017.00369.

O'Neill LAJ, Kishton RJ, Rathmell J. 2016. A guide to immunometabolism for immunologists. Nat Rev Immunol 16(9):553–565, PMID: 27396447, https://doi.org/10.1038/nri.2016.70.

O'Neill LA, Sheedy FJ, McCoy CE. 2011. MicroRNAs: the fine-tuners of Toll-like receptor signalling. Nat Rev Immunol 11(3):163–175, PMID: 21331081, https://doi.org/10.1038/nri2957.

Pakos-Zebrucka K, Koryga I, Mnich K, Ljujic M, Samali A, Gorman AM, et al. 2016. The integrated stress response. EMBO Rep 17(10):1374–1395, PMID: 27629041, https://doi.org/10.15252/embr.201642195.

Pan Z, Shan Q, Gu P, Wang XM, Tai LW, Sun M, et al. 2018. miRNA-23a/CXCR4 regulates neuropathic pain via directly targeting TXNIP/NLRP3 inflammasome axis. J Neuroinflamm 15(1):29, PMID: 29386025, https://doi.org/10.1186/s12974-018-1073-0.

Pestka J, Zhou HR. 2006. Toll-like receptor priming sensitizes macrophages to proinflammatory cytokine gene induction by deoxynivalenol and other toxicants. Toxicol Sci 92(2):445–455, PMID: 16687389, https://doi.org/10.1093/toxsci/kfl012.

Powers MF, Beavis AD. 1991. Triorganotins inhibit the mitochondrial inner membrane anion channel. J Biol Chem 266(26):17250–17256, PMID: 1716627, https://doi.org/10.1016/S0021-9258(19)47366-3.

Ralston JC, Lyons CL, Kennedy EB, Kirwan AM, Roche HM. 2017. Fatty acids and NLRP3 inflammasome-mediated inflammation in metabolic tissues. Annu Rev Nutr 37:77–102, PMID: 28826373, https://doi.org/10.1146/annurev-nutr-071816-064836.

Ramirez DC, Mason RP. 2005. Immuno-spin trapping: detection of protein-centered radicals. Curr Protoc Toxicol 24(1):17.7.1–17.7.18, PMID: 23045116, https://doi.org/10.1002/0471140856.tx1707s24.

Rebane A, Akdis CA. 2013. MicroRNAs: essential players in the regulation of inflammation. J Allergy Clin Immunol 132(1):15–26, PMID: 23726263, https://doi.org/10.1016/j.jaci.2013.04.011.

Redondo-Castro E, Faust D, Fox S, Baldwin AG, Osborne S, Haley MJ, et al. 2018. Development of a characterised tool kit for the interrogation of NLRP3 inflammasome-dependent responses. Sci Rep 8(1):5667, PMID: 29618797, https://doi.org/10.1038/s41598-018-24029-3.

Regala RP, Rice CD, Schwedler TE, Dorociak IR. 2001. The effects of tributyltin (TBT) and 3,3′,4,4′,5-pentachlorobiphenyl (PCB-126) mixtures on antibody responses and phagocyte oxidative burst activity in channel catfish, *Ictalurus punctatus*. Arch Environ Contam Toxicol 40(3):386–391, PMID: 11443370, https://doi.org/10.1007/s002440010187.

Ritchie ME, Phipson B, Wu D, Hu Y, Law CW, Shi W, et al. 2015. *limma* powers differential expression analyses for RNA-sequencing and microarray studies. Nucleic Acids Res 43(7):e47, PMID: 25605792, https://doi.org/10.1093/nar/gkv007.

Röhl C, Grell M, Maser E. 2009. The organotin compounds trimethyltin (TMT) and triethyltin (TET) but not tributyltin (TBT) induce activation of microglia co-

cultivated with astrocytes. Toxicol In Vitro 23(8):1541–1547, PMID: 19422909, https://doi.org/10.1016/j.tiv.2009.04.013.
Sandström J, Kratschmar DV, Broyer A, Poirot O, Marbet P, Chantong B, et al. 2019. In vitro models to study insulin and glucocorticoids modulation of trimethyltin (TMT)-induced neuroinflammation and neurodegeneration, and in vivo validation in db/db mice. Arch Toxicol 93(6):1649–1664, PMID: 30993381, https://doi.org/10.1007/s00204-019-02455-0.
Sanman LE, Qian Y, Eisele NA, Ng TM, van der Linden WA, Monack DM, et al. 2016. Disruption of glycolytic flux is a signal for inflammasome signaling and pyroptotic cell death. Elife 5:e13663, PMID: 27011353, https://doi.org/10.7554/eLife.13663.
Schindelin J, Arganda-Carreras I, Frise E, Kaynig V, Longair M, Pietzsch T, et al. 2012. Fiji: an open-source platform for biological-image analysis. Nat Methods 9(7):676–682, PMID: 22743772, https://doi.org/10.1038/nmeth.2019.
Schnitger AKD, Machova A, Mueller RU, Androulidaki A, Schermer B, Pasparakis M, et al. 2011. *Listeria monocytogenes* infection in macrophages induces vacuolar-dependent host miRNA response. PLoS One 6(11):e27435, PMID: 22114673, https://doi.org/10.1371/journal.pone.0027435.
Shaughnessy DT, McAllister K, Worth L, Haugen AC, Meyer JN, Domann FE, et al. 2014. Mitochondria, energetics, epigenetics, and cellular responses to stress. Environ Health Perspect 122(12):1271–1278, PMID: 25127496, https://doi.org/10.1289/ehp.1408418.
Sheedy FJ, Grebe A, Rayner KJ, Kalantari P, Ramkhelawon B, Carpenter SB, et al. 2013. CD36 coordinates NLRP3 inflammasome activation by facilitating intracellular nucleation of soluble ligands into particulate ligands in sterile inflammation. Nat Immunol 14(8):812–820, PMID: 23812099, https://doi.org/10.1038/ni.2639.
Shimada K, Crother TR, Karlin J, Dagvadorj J, Chiba N, Chen S, et al. 2012. Oxidized mitochondrial DNA activates the NLRP3 inflammasome during apoptosis. Immunity 36(3):401–414, PMID: 22342844, https://doi.org/10.1016/j.immuni.2012.01.009.
Sims JE, Smith DE. 2010. The IL-1 family: regulators of immunity. Nat Rev Immunol 10(2):89–102, PMID: 20081871, https://doi.org/10.1038/nri2691.
Snoeij NJ, Penninks AH, Seinen W. 1987. Biological activity of organotin compounds—an overview. Environ Res 44(2):335–353, PMID: 3319574, https://doi.org/10.1016/S0013-9351(87)80242-6.
Snoeij NJ, Penninks AH, Seinen W. 1988. Dibutyltin and tributyltin compounds induce thymus atrophy in rats due to a selective action on thymic lymphoblasts. Int J Immunopharmacol 10(7):891–899, PMID: 2466803, https://doi.org/10.1016/0192-0561(88)90014-8.
Snoeij NJ, van Iersel AAJ, Penninks AH, Seinen W. 1985. Toxicity of triorganotin compounds: comparative *in vivo* studies with a series of trialkyltin compounds and triphenyltin chloride in male rats. Toxicol Appl Pharmacol 81(2):274–286, PMID: 4060154, https://doi.org/10.1016/0041-008X(85)90164-4.
Sousa ACA, Pastorinho MR, Takahashi S, Tanabe S. 2014. History of organotin compounds, from snails to humans. Environ Chem Lett 12(1):117–137, https://doi.org/10.1007/s10311-013-0449-8.
Strowig T, Henao-Mejia J, Elinav E, Flavell R. 2012. Inflammasomes in health and disease. Nature 481(7381):278–286, PMID: 22258606, https://doi.org/10.1038/nature10759.
Stutz A, Horvath GL, Monks BG, Latz E. 2013. ASC speck formation as a readout for inflammasome activation. Methods Mol Biol 1040:91–101, PMID: 23852599, https://doi.org/10.1007/978-1-62703-523-1_8.
Swanson KV, Deng M, Ting JPY. 2019. The NLRP3 inflammasome: molecular activation and regulation to therapeutics. Nat Rev Immunol 19(8):477–489, PMID: 31036962, https://doi.org/10.1038/s41577-019-0165-0.
Taciak B, Białasek M, Braniewska A, Sas Z, Sawicka P, Kiraga Ł, et al. 2018. Evaluation of phenotypic and functional stability of RAW 264.7 cell line through serial passages. PLoS One 13(6):e0198943, PMID: 29889899, https://doi.org/10.1371/journal.pone.0198943.
Taetzsch T, Levesque S, McGraw C, Brookins S, Luqa R, Bonini MG, et al. 2015. Redox regulation of NF-κB p50 and M1 polarization in microglia. Glia 63(3):423–440, PMID: 25331559, https://doi.org/10.1002/glia.22762.
Tang X, Li N, Kang L, Dubois AM, Gong Z, Wu B, et al. 2013. Chronic low level trimethyltin exposure and the risk of developing nephrolithiasis. Occup Environ Med 70(8):561–567, PMID: 23703823, https://doi.org/10.1136/oemed-2012-101261.
Tannahill GM, Curtis AM, Adamik J, Palsson-McDermott EM, McGettrick AF, Goel G, et al. 2013. Succinate is an inflammatory signal that induces IL-1β through HIF-1α. Nature 496(7444):238–242, PMID: 23535595, https://doi.org/10.1038/nature11986.
Tezcan G, Martynova EV, Gilazieva ZE, McIntyre A, Rizvanov AA, Khaiboullina SF, et al. 2019. MicroRNA post-transcriptional regulation of the NLRP3 inflammasome in immunopathologies. Front Pharmacol 10:451, PMID: 31118894, https://doi.org/10.3389/fphar.2019.00451.
Tran UT, Kitami T. 2019. Niclosamide activates the NLRP3 inflammasome by intracellular acidification and mitochondrial inhibition. Commun Biol 2:2, PMID: 30740538, https://doi.org/10.1038/s42003-018-0244-γ.
Trinchieri G. 2003. Interleukin-12 and the regulation of innate resistance and adaptive immunity. Nat Rev Immunol 3(2):133–146, PMID: 12563297, https://doi.org/10.1038/nri1001.
Trouplin V, Boucherit N, Gorvel L, Conti F, Mottola G, Ghigo E. 2013. Bone marrow-derived macrophage production. J Vis Exp (81):e50966, PMID: 24300014, https://doi.org/10.3791/50966.
Tschopp J. 2011. Mitochondria: sovereign of inflammation? Eur J Immunol 41(5):1196–1202, PMID: 21469137, https://doi.org/10.1002/eji.201141436.
Tschopp J, Schroder K. 2010. NLRP3 inflammasome activation: the convergence of multiple signalling pathways on ROS production? Nat Rev Immunol 10(3):210–215, PMID: 20168318, https://doi.org/10.1038/nri2725.
Ueno S, Kashimoto T, Susa N, Asai T, Kawaguchi S, Takeda-Homma S, et al. 2009. Reduction in peripheral lymphocytes and thymus atrophy induced by organotin compounds *in vivo*. J Vet Med Sci 71(8):1041–1048, PMID: 19721355, https://doi.org/10.1292/jvms.71.1041.
Van Loveren H, Krajnc EI, Rombout PJA, Blommaert FA, Vos JG. 1990. Effects of ozone, hexachlorobenzene, and bis(tri-*n*-butyltin)oxide on natural killer activity in the rat lung. Toxicol Appl Pharmacol 102(1):21–33, PMID: 2136961, https://doi.org/10.1016/0041-008X(90)90080-E.
Vande Walle L, Van Opdenbosch N, Jacques P, Fossoul A, Verheugen E, Vogel P, et al. 2014. Negative regulation of the NLRP3 inflammasome by A20 protects against arthritis. Nature 512(7512):69–73, PMID: 25043000, https://doi.org/10.1038/nature13322.
Venegas C, Kumar S, Franklin BS, Dierkes T, Brinkschulte R, Tejera D, et al. 2017. Microglia-derived ASC specks cross-seed amyloid-β in Alzheimer's disease. Nature 552(7685):355–361, PMID: 29293211, https://doi.org/10.1038/nature25158.
Viola A, Munari F, Sánchez-Rodríguez R, Scolaro T, Castegna A. 2019. The metabolic signature of macrophage responses. Front Immunol 10:1462, PMID: 31333642, https://doi.org/10.3389/fimmu.2019.01462.
Wallace DC, Fan W. 2009. The pathophysiology of mitochondrial disease as modeled in the mouse. Genes Dev 23(15):1714–1736, PMID: 19651984, https://doi.org/10.1101/gad.1784909.
Walsh JG, Muruve DA, Power C. 2014. Inflammasomes in the CNS. Nat Rev Neurosci 15(2):84–97, PMID: 24399084, https://doi.org/10.1038/nrn3638.
West AP. 2017. Mitochondrial dysfunction as a trigger of innate immune responses and inflammation. Toxicology 391:54–63, PMID: 28765055, https://doi.org/10.1016/j.tox.2017.07.016.
Whalen MM, Loganathan BG, Kannan K. 1999. Immunotoxicity of environmentally relevant concentrations of butyltins on human natural killer cells *in vitro*. Environ Res 81(2):108–116, PMID: 10433842, https://doi.org/10.1006/enrs.1999.3968.
Wu B. 2019. Effects of trace elements—tin or tin compounds on animals. Austin J Vet Sci Anim Husb 6(2):1055. https://austinpublishinggroup.com/veterinary-science-research/fulltext/avsah-v6-id1055.pdf [accessed 12 April 2021].
Xia M, Huang R, Shi Q, Boyd WA, Zhao J, Sun N, et al. 2018. Comprehensive analyses and prioritization of Tox21 10K chemicals affecting mitochondrial function by in-depth mechanistic studies. Environ Health Perspect 126(7):077010, PMID: 30059008, https://doi.org/10.1289/EHP2589.
Zamani P, Oskuee RK, Atkin SL, Navashenaq JG, Sahebkar A. 2020. MicroRNAs as important regulators of the NLRP3 inflammasome. Prog Biophys Mol Biol 150:50–61, PMID: 31100298, https://doi.org/10.1016/j.pbiomolbio.2019.05.004.
Zhang QB, Qing YF, Yin CC, Zhou L, Liu XS, Mi QS, et al. 2018. Mice with miR-146a deficiency develop severe gouty arthritis via dysregulation of TRAF 6, IRAK 1 and NALP3 inflammasome. Arthritis Res Ther 20(1):45, PMID: 29544526, https://doi.org/10.1186/s13075-018-1546-7.
Zhang Y, Liu F, Yuan Y, Jin C, Chang C, Zhu Y, et al. 2017. Inflammasome-derived exosomes activate NF-κB signaling in macrophages. J Proteome Res 16(1):170–178, PMID: 27684284, https://doi.org/10.1021/acs.jproteome.6b00599.
Zheng D, Liwinski T, Elinav E. 2020. Inflammasome activation and regulation: toward a better understanding of complex mechanisms. Cell Discov 6:36, PMID: 32550001, https://doi.org/10.1038/s41421-020-0167-x.
Zhou R, Yazdi AS, Menu P, Tschopp J. 2011. A role for mitochondria in NLRP3 inflammasome activation. Nature 469(7329):221–225, PMID: 21124315, https://doi.org/10.1038/nature09663.
Zhou Y, Lu M, Du RH, Qiao C, Jiang CY, Zhang KZ, et al. 2016. MicroRNA-7 targets Nod-like receptor protein 3 inflammasome to modulate neuroinflammation in the pathogenesis of Parkinson's disease. Mol Neurodegener 11:28, PMID: 27084336, https://doi.org/10.1186/s13024-016-0094-3.
Zhu S, Pan W, Song X, Liu Y, Shao X, Tang Y, et al. 2012. The microRNA miR-23b suppresses IL-17-associated autoimmune inflammation by targeting TAB2, TAB3 and IKK-α. Nat Med 18(7):1077–1086, PMID: 22660635, https://doi.org/10.1038/nm.2815.